Magnetic helicity in magnetohydrodynamic turbulence with a mean magnetic field

Troy Stribling, William H. Matthaeus, and Sean Oughton

Citation: Physics of Plasmas (1994-present) **2**, 1437 (1995); doi: 10.1063/1.871359
View online: http://dx.doi.org/10.1063/1.871359
View Table of Contents: http://scitation.aip.org/content/aip/journal/pop/2/5?ver=pdfcov
Published by the AIP Publishing

Magnetic helicity in magnetohydrodynamic turbulence with a mean magnetic field

Troy Stribling
National Research Council, NASA Goddard Space Flight Center, Greenbelt, Maryland 20771

William H. Matthaeus and Sean Oughton
Bartol Research Institute, University of Delaware, Newark, Delaware 19716

(Received 20 May 1994; accepted 20 January 1995)

A computational investigation of magnetic helicity of the fluctuating magnetic field H_m in ideal and freely decaying three-dimensional (3-D) magnetohydrodynamics (MHD) in the presence of a uniform mean magnetic field is performed. It is shown that for ideal 3-D MHD H_m, which is a rugged invariant in the absence of a mean magnetic field [Frisch *et al.*, J. Fluid Mech. **77**, 796 (1975)], decays from its initial value and proceeds to oscillate about zero. The decay of H_m is shown to result from the presence of a new "generalized" helicity invariant, which includes contributions from the uniform magnetic field. The loss of invariance of H_m will diminish the effects of inverse transfer of H_m on freely decaying turbulence. This is demonstrated in a discussion of the selective decay relaxation process. © *1995 American Institute of Physics.*

I. INTRODUCTION

The magnetic helicity (H_m) of the fluctuating magnetic field is a measure, which has proven important in the description of mirror asymmetric three-dimensional (3-D) magnetohydrodynamic (MHD) turbulence.[1–10] For a turbulent magnetic field H_m may be defined by

$$H_m=\langle \mathbf{a}\cdot\mathbf{b}\rangle, \tag{1}$$

where $\mathbf{b}$ is the fluctuating magnetic field, $\mathbf{b}=\nabla\times\mathbf{a}$ defines the vector potential $\mathbf{a}$ and $\langle\cdots\rangle$ denotes a spatial average over a volume of interest. Here both $\mathbf{b}$ and $\mathbf{a}$ have zero means, and it is convenient to adopt the Coulomb gauge in which $\nabla\cdot\mathbf{a}=0$. Magnetic helicity can be interpreted, as suggested by Moffatt,[11] as a measure of linkage of magnetic flux tubes. Also, if one Fourier transforms $\mathbf{b}$, with the Fourier coefficients indexed by wave number $\mathbf{k}$, then H_m measures the polarization of the $\mathbf{b}(\mathbf{k})$. Plane polarized $\mathbf{b}(\mathbf{k})$ have zero H_m and circularly polarized $\mathbf{b}(\mathbf{k})$ have a maximal value of H_m whose magnitude is equal to $|\mathbf{b}(\mathbf{k})|^2/k$. The average polarization measures the correlation between independent components of $\mathbf{b}(\mathbf{k})$ as well. For MHD turbulence the second interpretation is the most convenient.

The significance of H_m in turbulence theory arises because it is conserved in the absence of Ohmic dissipation for a variety of boundary conditions. This conservation law is central in the arguments given by Frisch and co-workers for the inverse cascade phenomenon in three-dimensional incompressible MHD turbulence,[1] an effect that is driven by spectral transfer of H_m to long wavelengths. This "back-transfer" of H_m to long wavelengths has been cited as a contributor to efficient magnetic dynamo activity in forced[2,8] and freely decaying MHD.[4,7] In freely decaying MHD turbulence, relaxation through the selective decay process occurs because H_m is back-transferred to long wavelengths where dissipation is weak.[3,5,9,12] In these theoretical treatments the invariance of magnetic helicity in the absence of dissipation is crucial. However, these arguments have generally been developed for magnetofluids that are, in effect, *isolated*, through the use of perfectly conducting boundary conditions, or the use of periodic boundary conditions. For these cases, magnetic field lines either do not leave the volume containing the turbulence, or, for the periodic case, close in a finite region of space.

Concepts developed in homogeneous MHD turbulence theory are usually applied to local parcels of turbulent plasma fluid, particularly in space physics and astrophysics. In these applications, externally supported magnetic fields can thread the parcel without closing in this region. This alternative situation may eventually prove to be more relevant than the case of "isolated" homogeneous turbulence, which is often modeled using periodic boundary conditions with a zero volume-averaged magnetic field. Here we examine the case where the volume is threaded by a uniform eternally generated magnetic field. An investigation of magnetic helicity in a MHD model with a uniform magnetic field might prove relevant for interplanetary applications. In particular, MHD scale turbulence in the solar wind is frequently modeled in terms of homogeneous turbulence theory,[13] motivating models using periodic boundaries. However, interplanetary space also contains the large-scale solar magnetic field, which appears locally (on the scale of a correlation length) as a uniform field. Fluctuations in H_m have been observed in the solar wind.[13–15] The inertial range fluctuations in these observations have been shown to be randomly distributed with zero mean, although there is evidence for a net magnetic helicity at the energy containing fluctuation scale.[16,17] It is also believed that H_m plays a role in cosmic ray transport in the heliosphere.[15,16]

Important connections also exist between the behavior of magnetic helicity in a homogeneous plasma parcel and analogous effects in mean field electrodynamics,[11,18–20] which seeks to determine effects of local fluctuations on large-scale fields in an inhomogeneous magnetofluid. While this leads to important effects in space and the astrophysical dynamo theory,[20] we will focus, at present, entirely on the homogeneous model problem.

For a homogeneous parcel of MHD turbulence threaded by a uniform magnetic field H_m, defined by Eq. (1), is no longer an invariant in ideal MHD. Instead, a more general definition for magnetic helicity, which includes a contribution from the uniform magnetic field, becomes an ideal invariant,[13] if the boundary condition is appropriately defined, for example, perfectly conducting-free-slip or periodic. This invariant is a generalization of the fluctuation magnetic helicity H_m, which we designate as the modified magnetic helicity of the fluctuations, denoted by $\hat{H}_m$, it is given by

$$\hat{H}_m = H_m + 2\mathbf{B}_0 \cdot \mathbf{A}_0, \tag{2}$$

where H_m is defined by Eq. (1). The quantity $d\mathbf{A}_0/dt = \langle \mathbf{v} \times \mathbf{b} \rangle = -\mathbf{E}_0$ is the negative of the volume-averaged-induced electric field, and can be interpreted as the time derivative of the $\mathbf{k}=0$ component of the vector potential. However, note that $\nabla \times \mathbf{A}_0 = 0 \neq \mathbf{B}_0$, and even ignoring this fact, $\hat{H}_m$ is not the magnetic helicity one would compute using Eq. (1) and including the direct current (DC) contributions $\mathbf{A}_0$ and $\mathbf{B}_0$. The result so obtained would differ from $\hat{H}_m$ by an amount $\mathbf{B}_0 \cdot \mathbf{A}_0$. One possible interpretation of the $\mathbf{B}_0 \cdot \mathbf{A}_0$ term of $\hat{H}_m$ is that it represents magnetic flux linkages produced by scales much larger than the periodicity length of $\mathbf{b}$.[11,13]

We caution, however, that $\hat{H}_m$ cannot, in any sense, be thought of as the *total* magnetic helicity, which would need also to take in to account the vector potential that gives rise to $\mathbf{B}_0$. In Ref. 18 we discuss the relationship of periodic turbulence to scale-separated turbulence with a slowly varying large-scale magnetic field $\mathbf{B}_0$. While this development supports some of the above interpretations of $\hat{H}_m$, it also shows that there is a slowly varying nonperiodic vector potential $\mathbf{A}^{(-1)}$ that provides the source for $\mathbf{B}_0$. Considering the *total* magnetic helicity in the system, one would include a (non-normalized) contribution $\int d^3x\, \mathbf{B}_0 \cdot \mathbf{A}^{(-1)}$, which is entirely unaccounted for in the definition of $\hat{H}_m$ [Eq. (2)]. We shall not attempt in this paper to discuss matters pertaining to the total system magnetic helicity. Rather, we concentrate on H_m and $\hat{H}_m$, noting that H_m is itself gauge invariant, while $\hat{H}_m$ is completely specified by choosing an (arbitrary) value of $\mathbf{A}_0$ at $t=0$ and advancing it according to the uniquely defined rule given below Eq. (2). No gauge transformations apply to $\hat{H}_m$ for the problem at hand, since there is no magnetic field in this problem, which is obtained by differentiating $\mathbf{A}_0$. Therefore all quantities of interest here are fully and uniquely determined, but we can say nothing about the large-scale problem or about the total magnetic helicity.

Invariance of magnetic helicity in ideal MHD is central to past theoretical investigations of the dynamics mirror asymmetric homogeneous turbulence.[1–7] The loss of this conservation law for the more general system that is threaded by a mean magnetic field motivates this reexamination of the dynamics of a turbulent helical magnetofluid. In this paper we examine the dynamical properties of H_m for a simple model, in which the MHD turbulence is periodic, but evolves in the presence of a specified, externally supported uniform magnetic field. We show, by considering the helicity conservation law, Eq. (1), and by use of the direct numerical solution of the three-dimensional (3-D) MHD equations, see Sec. II, that helicity behaves dynamically in a different way than in the case of magnetically isolated MHD turbulence.

Our principal purpose here is to examine how the change from nondissipative invariance of H_m to invariance of $\hat{H}_m$ when $B_0 \neq 0$ influences the character of the turbulence. We examine both dissipative and nondissipative simulations. With regard to the behavior of the magnetic helicity itself, for the ideal case there would appear to be three possibilities, which have not been distinguished in the previous literature as far as we are aware. Focusing on the nonlinear nondissipative evolution of $\hat{H}_m$, first, the new term $\mathbf{B}_0 \cdot \mathbf{A}_0$ might tend to average to zero over time, a possibility that might not produce great changes to mechanisms that depend upon inverse transfer processes. Second, one could suspect that $\mathbf{B}_0 \cdot \mathbf{A}_0$ might tend to become statistically equipartitioned with H_m, with concomitant effects on spectral transfer. Finally, H_m might decay in favor of $\mathbf{B}_0 \cdot \mathbf{A}_0$. This outcome would lead to the most drastic changes in the dynamics of homogeneous MHD turbulence, since it could significantly diminish H_m back-transfer tendencies. The difficulty in distinguishing these possible outcomes on the basis of theoretical arguments is compounded by the nature of the new ideal conservation law, which is of a type that differs from previous experience with rugged invariants in MHD. Specifically, one easily sees that the time evolution of $\mathbf{B}_0 \cdot \mathbf{A}_0$ depends upon the *time history* of the turbulence, since $\mathbf{A}_0(\mathbf{x},t) = \mathbf{A}_0(\mathbf{x},0) - \int_0^t \mathbf{E}_0(\mathbf{x},t')\,dt'$. Consequently, we have appealed to numerical simulations to provide guidance, arriving at the conclusion that the third possibility cited above best describes the tendencies seen in both dissipative and nondissipative 3-D incompressible MHD flows. A preliminary report of this finding was presented recently.[18] Here we will present further numerical and analytical investigation of this dynamical process, which amounts to a nonlinear decay of the magnetic helicity content of the fluctuations. In Sec. IV we present a series of nondissipative simulations that survey the nonlinear decay of H_m. Also, in Sec. IV an absolute equilibrium theory is presented that accurately describes the time-averaged properties of the ideal simulations. This absolute equilibrium theory is constructed, assuming $\hat{H}_m$ to be a statistically nonisolating[21] invariant.

Having seen that the magnetic helicity itself can behave quite differently when there is an applied DC magnetic field, we will turn to an investigation of the complications that this produces in understanding dissipative relaxation processes in MHD. In Secs. V and VI the consequences of the ideal nonlinear H_m decay process are described by appeal to freely decaying MHD simulations. In particular, we discuss the influence of this process on the selective decay and dynamic alignment relaxation processes. We find that the ideal H_m decay processes can have a very significant negative influence on H_m back-transfer effects, such as the selective decay relaxation process. This result suggests that modifications to the theory of the dynamics of helical MHD turbulence are necessary when the system is threaded by an externally generated magnetic field.

II. MHD EQUATIONS AND RUGGED INVARIANTS

We perform an investigation of constant density unforced 3-D MHD, which, written in Alfvén speed units, has the form

$$\frac{\partial \mathbf{v}}{\partial t}+\mathbf{v}\cdot\nabla\mathbf{v}=-\nabla p^*+\mathbf{b}\cdot\nabla\mathbf{b}+\mathbf{B}_0\cdot\nabla\mathbf{b}+\nu\,\nabla^2\mathbf{v}, \tag{3}$$

$$\frac{\partial \mathbf{b}}{\partial t}+\mathbf{v}\cdot\nabla\mathbf{b}=\mathbf{b}\cdot\nabla\mathbf{v}+\mathbf{B}_0\cdot\nabla\mathbf{v}+\eta\,\nabla^2\mathbf{b}, \tag{4}$$

$$\nabla\cdot\mathbf{v}=0, \tag{5}$$

$$\nabla\cdot\mathbf{b}=0. \tag{6}$$

The fluctuating velocity and magnetic fields, $\mathbf{v}$ and $\mathbf{b}$, each have zero mean, $\mathbf{B}_0$ is the mean magnetic field, which is assumed to be uniform, p^* is the total pressure, determined by a Poisson equation when use is made of the incompressibility equation (4), and ν and η are the viscosity and resistivity, respectively. The time unit is taken to be an eddy turnover time for the unit velocity field at a unit length scale. In this work simulations are discussed in which ν and η are taken to be 0.01 and zero. The numerical solution of Eqs. (2)–(5) will assume periodic boundary conditions in a cube with sides of length 2π. The fluctuating velocity and magnetic fields $\mathbf{v}$ and $\mathbf{b}$ are represented by discrete Fourier series, namely,

$$\mathbf{v}(\mathbf{x},t)=\sum_{\mathbf{k}\in\mathbf{M}}\mathbf{v}(\mathbf{k},t)\exp(i\mathbf{k}\cdot\mathbf{x}), \tag{7}$$

$$\mathbf{b}(\mathbf{x},t)=\sum_{\mathbf{k}\in\mathbf{M}}\mathbf{b}(\mathbf{k},t)\exp(i\mathbf{k}\cdot\mathbf{x}), \tag{8}$$

where $\mathbf{M}$ is a collection of 3-D wave vectors $\mathbf{k}$ with integer components, such that $k_{\min}\leqslant|\mathbf{k}|\leqslant k_{\max}$. The simulations discussed in the following sections have either 8^3 or 32^3 wave numbers.

Of particular importance in this work are quantities known as rugged invariants. These invariants are conserved by arbitrary truncations of the Galerkin representations of Eqs. (3)–(6), and are statistically isolating, in the sense that they determine the phase space volume occupied by the inviscid system in a statistical mechanics analysis.[22] When $\mathbf{B}_0=0$ there are believed to be only three rugged invariants.[1,6] They are the total energy, cross-helicity, and magnetic helicity. For periodic 3-D MHD the rugged invariants are explicitly given by

$$E=\frac{1}{2V}\int|\mathbf{v}|^2+|\mathbf{b}|^2\,d^3x=E_v+E_b, \tag{9}$$

$$H_c=\frac{1}{2V}\int\mathbf{v}\cdot\mathbf{b}\,d^3x, \tag{10}$$

$$H_m=\frac{1}{V}\int\mathbf{a}\cdot\mathbf{b}\,d^3x, \tag{11}$$

where $V=8\pi^3$. Each rugged invariant is expressed as a per unit mass quantity, and the integrals are evaluated over a cube with sides of length 2π. The cross-helicity can be viewed as a measure of correlation between the velocity magnetic fields, and possible interpretations of H_m were previously mentioned.

In this work we are primarily concerned with the $B_0\neq0$ case. Numerical simulations of inviscid 3-D MHD with a nonzero $\mathbf{B}_0$ are presented in Sec. IV, which suggest that the total energy and cross-helicity remain rugged invariants. The magnetic helicity defined by Eq. (1), with $\langle\mathbf{b}\rangle=0$, is not a rugged invariant, as in the $B_0=0$ case. Instead, as previously mentioned, the modified magnetic helicity of the fluctuations $\hat{H}_m$, defined by Eq. (2), is an ideal invariant. In our ideal simulations we find that this quantity is constant in time. Though it is an ideal constant of motion, our results suggest that it may not be a statistically isolating, rugged invariant. In Sec. IV data will be presented to support this hypothesis.

III. NUMERICAL PROCEDURES

The incompressible 3-D MHD code assumes periodic boundary conditions in each spatial dimension. Spatial discretization is performed with a Fourier spectral algorithm, which uses isotropic truncation to remove aliasing errors.[23] A second-order Adams–Bashforth method is used for time integration of the nonlinear terms, and the diffusive terms are integrated with a Crank–Nicholson method. The errors in conservation of the rugged invariants for this method are due solely to the time integration method, and can be controlled by adjusting the time step.

Simulations are performed with both 8^3 and 32^3 Fourier modes. Each of the 8^3 simulations are ideal, i.e., $\eta=\nu=0$. These ideal simulations are used to investigate the time evolution of H_m and $\hat{H}_m$, and to study long time averages of various modal and global quantities. It is felt that the low spatial resolution of these simulations is not prohibitive for this type of analysis.[24] Also, the low spatial resolution permits very long time integration, and the performance of numerous simulations. The collection of 8^3 runs samples the two-dimensional parameter space spanned by H_c and B_0, which have a significant effect on the H_m decay rate in ideal MHD. The initial conditions for these simulations have the following form. The total energy and cross-helicity spectra are flat for $1\leqslant|\mathbf{k}|\leqslant3$, and zero otherwise. Over the range of excited wave numbers, the Alfvén ratio is given by $E_v(\mathbf{k})/E_b(\mathbf{k})=1$, and the dimensionless magnetic helicity spectrum $\sigma_m(\mathbf{k})=H_m(\mathbf{k})k/E_b(\mathbf{k})$ is flat. Here $E_v(\mathbf{k})$, $E_b(\mathbf{k})$, and $H_m(\mathbf{k})$ are the kinetic energy, magnetic energy, and magnetic helicity spectra, respectively. The global values of the total energy, Alfvén ratio, and magnetic helicity are $E=1$, $E_v/E_b=1$, and $H_m=0.2$. Also, for each simulation the RMS fluctuating magnetic field $\sqrt{\langle|\mathbf{b}|^2\rangle}$ has unit magnitude. The mean magnetic field is always specified to lie along the $\hat{\mathbf{z}}$ direction. All other properties of the fields are randomly determined. The time step for each simulation is $\Delta t=10^{-2}$ and the integration is performed out to a minimum of 3000 time steps or 30 eddy turnover times, and a maximum of 120 000 time steps or 1200 turnover times. In the longest run, energy is conserved to four significant figures.

Seven 32^3 simulations are discussed. Six of the runs are dissipative with $\eta=\nu=0.01$, and one is ideal. In the dissipa-

tive simulations, 32^3 wave numbers is sufficient for resolution of all the dynamically important length scales. The initial condition for each of the runs has the following form. The total energy and cross-helicity spectra are flat for $1 \leq |\mathbf{k}| \leq 5$, and zero otherwise. Over the range of excited wave numbers, $E_v(\mathbf{k})/E_b(\mathbf{k}) = 1$ and $\sigma_m(\mathbf{k})$ is flat. Also, global values of the total energy, Alfvén ratio, and magnetic helicity are $E = 1$, $E_v/E_b = 1$, and $H_m = 10^{-1}$. For each run $\mathbf{B}_0$ is assumed to lie along the $\hat{\mathbf{z}}$ direction, and the magnitude of the mean magnetic field B_0 and H_c are varied. All other properties of the fields are randomly determined.

The ideal 32^3 simulation is used to verify that the 8^3 results on the ideal H_m decay process are not qualitatively different for larger systems. It also allows comparison with the dissipative simulations, so that the influence of a nonzero resistivity and viscosity on the process can be determined. This simulation was integrated for 10 000 time steps with $\Delta t = 10^{-3}$, which corresponds to ten eddy turnover times. The magnitude of $\mathbf{B}_0$ is taken to be one and $H_c = 10^{-3}$. The total energy was conserved to four significant figures for this simulation.

The six dissipative 32^3 simulations are divided into two groups. One group scans the low H_c portion of the $B_0 - H_c$ parameter space, and the other the high H_c portion. For each of the two groups we perform simulations with $B_0 = 0$, $B_0 < \sqrt{\langle |\mathbf{b}|^2 \rangle}$, and $B_0 = \sqrt{\langle |\mathbf{b}|^2 \rangle}$. The initial condition for each of the three runs in a group are identical. The three runs are compared to determine the effect of the nonlinear H_m decay process on the selective decay and dynamic alignment relaxation processes, as the magnitude of $\mathbf{B}_0$ is varied. Also, the group of low H_c simulations has the same initial condition as the ideal run. These simulations are compared to investigate the effect of resistivity on the nonlinear H_m decay process. For each dissipative simulation $\Delta t = 10^{-2}$ and time integration is carried out to 30 000 time steps or 30 eddy turnover times at unit velocity. The 32^3 simulations require 1.5 s of computer time per time step on a Cray-YMP.

IV. IDEAL SIMULATIONS

The study of inviscid fluid systems has played an important role in the development of turbulence theory, most likely, because of the ease with which these systems yield to a rigorous statistical theory, in contrast to high Reynolds number dissipative flows. An interest in the statistical theories of inviscid fluid systems began after Lee[25] showed that Galerkin representations of these systems satisfy a Liouville theorem in the solution space. This led to the paradigm of constructing absolute equilibrium ensembles, i.e., canonical ensembles, upon identifying the statistically isolating, or "rugged," invariants of motion.[26] An aspect of the study of absolute equilibrium ensembles that has proven important to the theory of high Reynolds number turbulence are the inferences concerning direction of transfer of the rugged invariants in wave number space.[1,3,6,26,27]

In 3-D MHD without a mean magnetic field, the magnetic helicity spectrum experiences a *Bose-like* condensation in the longest wavelengths of the system when the dimension of the phase space is taken to infinity while keeping the rugged invariants constant.[1,6] For a finite-dimensional phase space, large peaks occur in the H_m spectrum in the longest wavelength. It has been proposed that this property of the absolute equilibrium H_m spectrum may be responsible for back-transfer of magnetic helicity in high Reynolds number MHD flows.[1] Back-transfer of H_m leads to its inverse cascade in forced MHD, which has been observed in numerical solutions of EDQNM closures.[2] For freely decaying 3-D MHD turbulence H_m back-transfer has been invoked as the dynamical mechanism, leading to selective decay relaxation,[3] which was developed to explain some properties of reverse-field pinch plasma devices.[9] Also, for freely decay MHD it has been suggested that H_m back-transfer can significantly slow down the energy decay rate.[7]

As previously mentioned, when a mean magnetic field is present, H_m is no longer conserved. Instead a generalized magnetic helicity, which we refer to as $\hat{H}_m$ defined by Eq. (2), becomes an invariant. In this section the results of several inviscid simulations are discussed. We find that indeed $\hat{H}_m$ is a constant in time, and that its invariance allows a nonlinear process that leads to the destruction of the magnetic helicity of the fluctuating magnetic field [i.e., H_m; see Eq. (1)] initially in the system. The nonlinear process, in addition to causing the decay of H_m, leads the production of a transient electric field aligned with the mean magnetic field.[18] This effect could have a strong influence on high Reynolds number turbulence processes that are believed driven by the back-transfer of H_m to low wave numbers. In Secs. IV D and V, this topic will be taken up in more detail. The time scale for the nonlinear H_m decay process is shown to vary with the value of the mean magnetic field and cross-helicity. Simulations are performed to qualitatively map out the dependence on these two parameters. Long time averages of global and spectral quantities are computed and compared with an absolute equilibrium theory. The results of this comparison suggest that $\hat{H}_m$ may not be a statistically isolating invariant.

A. Nonlinear decay of magnetic helicity

Each of the contributions to $\hat{H}_m$ from an 32^3 ideal simulation is given in Fig. 1. For this particular run, $\mathbf{B}_0 = 1\hat{\mathbf{z}}$, $\sqrt{\langle |\mathbf{b}|^2 \rangle}/B_0 = 1$, $E = 1$, $H_c = 10^{-3}$, and at $t = 0$, $H_m = 0.1$. The time history of H_m is given in Fig. 1(a). It is seen that H_m decays very quickly to zero while $\hat{H}_m$ remains constant; see Fig. 1(d). In Fig. 1(b) the time history of the $\hat{\mathbf{z}}$ component of spatially averaged electric field $E_{0z} = -1/V \int (\mathbf{v} \times \mathbf{b})_z \, d^3x$ is given. Only the $\hat{\mathbf{z}}$ component of $\mathbf{E}_0$, which in the simulations lies along $\mathbf{B}_0$, enters into $\hat{H}_m$. Most noticeable is the pulse in E_{0z}, which coincides with the period of most rapid decay in H_m. The time integral of E_{0z}, the $\hat{\mathbf{z}}$ component of $\mathbf{A}_0$, is depicted in Fig. 1(c). The pulse in E_{0z} gives rise to rapid growth in A_{0z}, which signifies the conversion of H_m into $\mathbf{B}_0 \cdot \mathbf{A}_0$. Because $\hat{H}_m$ is conserved during this process, the fluctuations in E_{0z} are perfectly anticorrelated with the dH_m/dt fluctuations.

An interesting consequence of the conservation of $\hat{H}_m$ and the subsequent decay of H_m is the production of a transient E_{0z} that persists while H_m is decaying most rapidly. Some properties of the E_{0z} pulse can be seen from an exami-

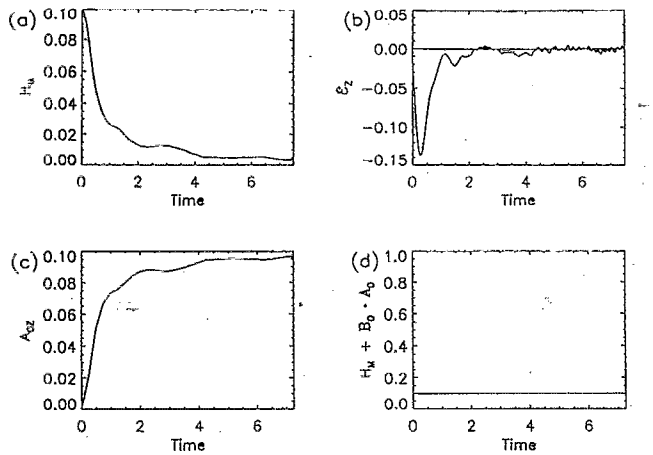

FIG. 1. Time histories of contributions to $\hat{H}_m$ [see Eq. (2)] for a 32^3 ideal simulation. For this run $E=1$, $H_c=10^{-3}$, and at $t=0$, $H_m=0.1$. The curves in each panel are (a) the time history of the fluctuating magnetic helicity H_m, (b) the time history of the $\hat{\mathbf{z}}$ component of the volume-averaged electric field E_{0z}, (c) the time history of the $\hat{\mathbf{z}}$ component of the volume-averaged vector potential A_{0z} (this curve is the time integral of E_{0z}), and (d) the time history of modified fluctuation magnetic helicity $\hat{H}_m$.

nation of the definition of $\hat{H}_m$. First, assume that $H_m(t=0)>0$. Now, since H_m decays as time progresses, to conserve $\hat{H}_m$ the $\mathbf{B}_0\cdot\mathbf{A}_0$ term must be positive and increasing while H_m is decreasing. This, in turn, requires that the component of the electric field along $\mathbf{B}_0$ to have the sign opposite of $\mathbf{B}_0$ as H_m decreases (recall that $d\mathbf{A}_0/dt=-\mathbf{E}_0$). In a similar vein, if $H_m(t=0)<0$, then a transient mean parallel electric field is generated in the same direction of $\mathbf{B}_0$. In Fig. 1(b), initial values of E_{0z} and H_m are negative and positive, respectively. In accordance with the conservation of $\hat{H}_m$ a E_{0z} in the direction opposite $\mathbf{B}_0$ is concurrent with the initial period of decay of H_m. In Fig. 2 the time history of E_{0z} for an 8^3 simulation is given. For this simulation the initial values of E_{0z} and H_m are negative and positive, respectively, and $\mathbf{B}_0$ is in the negative $\hat{\mathbf{z}}$ direction. In this initial configuration for H_m to decay and conserve $\hat{H}_m$, a transient E_{0z} in the positive $\hat{\mathbf{z}}$ direction is necessary. Thus, in Fig. 2, E_{0z} is seen to reverse sign from its initial value and produce the

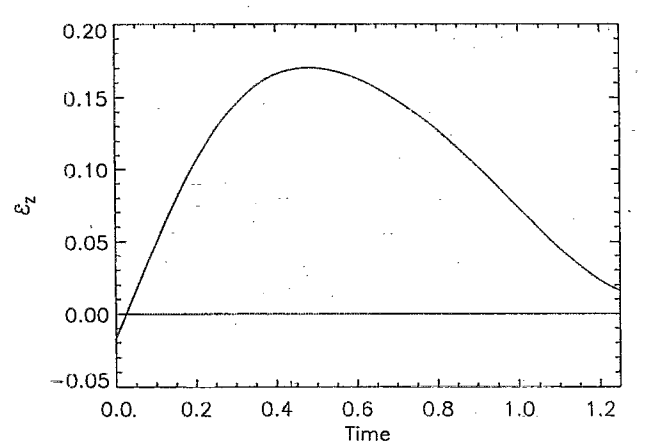

FIG. 2. The time history of the $\hat{\mathbf{z}}$ component of volume-averaged electric field E_{0z} for an 8^3 ideal simulation.

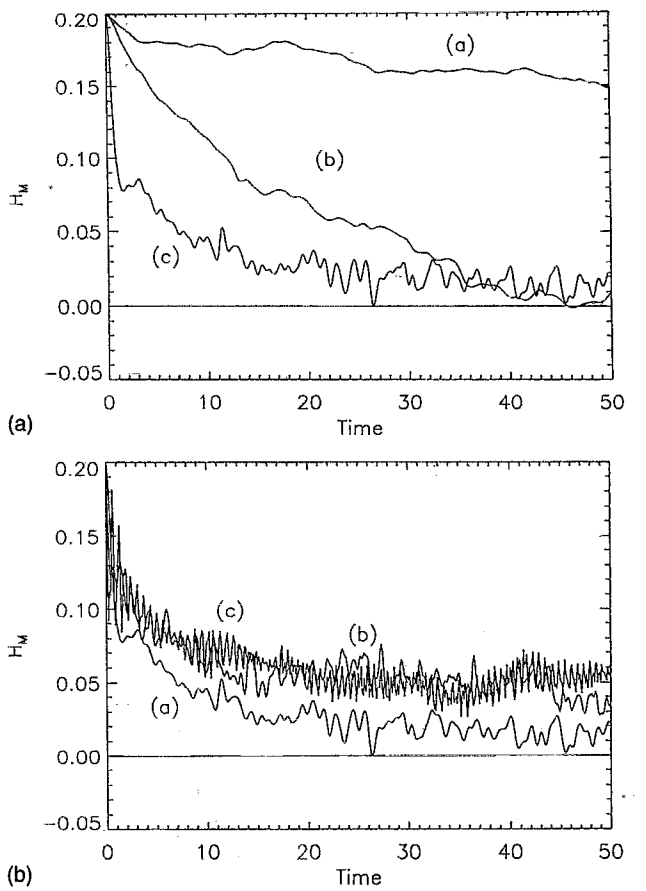

FIG. 3. Time histories of the fluctuating magnetic helicity H_m for a series of 8^3 ideal simulations. This set of curves illustrates the dependence of the nonlinear H_m decay rate on B_0. The cross-helicity H_c is 0.2 and $\sqrt{\langle|\mathbf{b}|^2\rangle}=1$ in each of the simulations. In panel (a) B_0 takes on the values (a) 0.1, (b) 0.2, and (c) 1. In panel (b) B_0 takes on the values (a) 1, (b) 2, and (c) 5.

requisite pulse. Also, though not shown, for the brief period that E_{0z} was negative in this simulation, H_m slightly increased, in accordance with the conservation law. This suggests that the more probable configuration of the system is one that will allow the decay of H_m.

We find that the decay rate of H_m depends quite strongly on the parameters H_c and $\sqrt{\langle|\mathbf{b}|^2\rangle}/B_0$. There are possibly other parameters that could cause a significant change in the decay rate of H_m, such as the number of Fourier modes kept in the truncation and the shape of the initial H_m spectrum, but because of limitations in computational resources we are unable to carry out a complete investigation of the conceivable parameter space. Thus, we chose to restrict these initial investigations to just the dependence on H_c and B_0, since they are most likely the most important parameters, because H_c is a rugged invariant and a nonzero B_0 is necessary for the operation of the decay process. A series of 8^3 dissipationless simulations was performed that samples H_c and $\sqrt{\langle|\mathbf{b}|^2\rangle}/B_0$ parameter space. In the two plots of Fig. 3, the time history of H_m is shown as $\sqrt{\langle|\mathbf{b}|^2\rangle}/B_0$ is varied, while H_c is held fixed at 0.2. For all runs, $H_m=0.2$ initially and $\sqrt{\langle|\mathbf{b}|^2\rangle}=1$. In Fig. 3(a), B_0 takes on the values (a) 0.1, (b) 0.2, and (c) 1, and in Fig. 3(b) the values (a) 1, (b) 2, and (c) 5. The decay rate of H_m is seen to increase as B_0 increases in

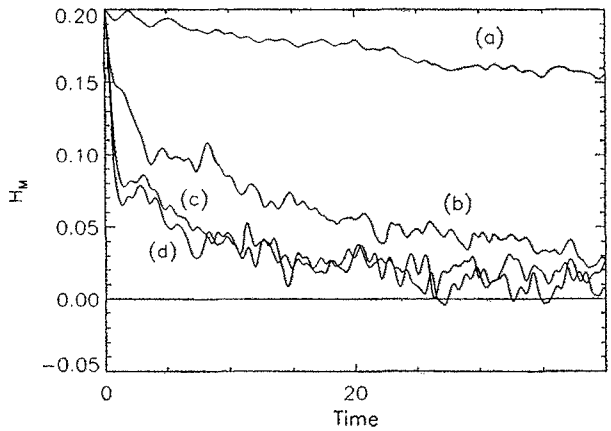

FIG. 4. The time histories of the fluctuating magnetic helicity H_m for a series of 8^3 ideal simulations. This set of curves illustrates the dependence of the nonlinear H_m decay rate on the cross-helicity H_c. For each simulation $\sqrt{\langle|\mathbf{b}|^2\rangle}/B_0 = 1$. The value of H_c for each curve is (a) 0.49, (b) 0.4, (c) 0.2, and (d) 0.001.

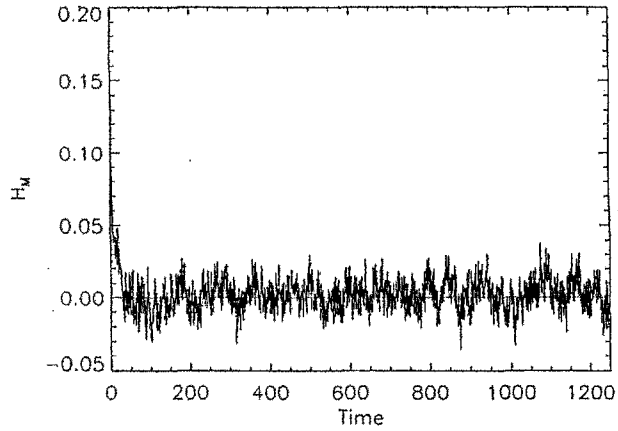

FIG. 5. The time history of fluctuating magnetic helicity H_m for an ideal 8^3 simulation integrated out to 1200 eddy turnover times. This figure illustrates the fluctuating character of H_m at long times. The correlation time for this curve is approximately eight eddy turnover times.

Fig. 3(a), while in Fig. 3(b) it decreases as B_0 continues to increase. Thus, it seems that a maximum exists in the H_m decay rate as a function of $\sqrt{\langle|\mathbf{b}|^2\rangle}/B_0$. From the figures this maximum appears to be near $B_0=1$ (i.e., $B_0 = \sqrt{\langle|\mathbf{b}|^2\rangle}$), a possible qualitative explanation of this behavior is as follows. For infinite Alfvén speed, $B_0=0$, H_m is conserved, so for H_m to decay a finite Alfvén speed is required. But decreasing the Alfvén speed causes the spectral transfer time scale to increase,[28,29] leading to a slowdown of the nonlinear interactions between Fourier modes. It is possible that competition between these two effects leads to the maximum rate of decay.

The time history of H_m for the collection of runs that sample the H_c portion of the parameter space is shown in Fig. 4. For these four runs, $B_0 = \sqrt{\langle|\mathbf{b}|^2\rangle}$ and $H_m=0.2$ initially, and H_c has the values (a) 0.49, (b) 0.4, (c) 0.2, and (d) 0.01. Kinematic constraints on H_c require it to satisfy the inequality $|H_c| \leq \frac{1}{2}E$. From Fig. 4 the decay rate of H_m is seen to decrease as H_c increases. This behavior is anticipated because increasing H_c is known to increase the time scale for spectral transfer.[29,30] In fact, for perfectly correlated $\mathbf{v}$ and $\mathbf{b}$, the nonlinear terms in the MHD equations cancel [see Eqs. (3) and (4)].

B. Time asymptotic properties

In this section long time averages and other properties of an ideal 8^3 simulation integrated out to 1200 eddy turnover times are presented. In an investigation of this type, long time series are necessary because we wish to compare the results with the ensemble-averaged absolute equilibrium theory predictions in the following section. Limitations in computational resources therefore restrict our study to a rather small 8^3 system. This should not pose any great restrictions, since for small systems the absolute equilibrium theory is thought to give accurate results for low-order moments.[24,6]

As previously discussed, a consequence of the presence of $\mathbf{B}_0$ is to cause H_m to decay and begin to fluctuate about zero. After an examination of several simulations with different values of $\mathbf{B}_0$, it is our belief that the time asymptotic properties of the inviscid system are independent of this parameter. The way $\mathbf{B}_0$ is felt time asymptotically appears to be by elimination of rugged invariance H_m. The magnitude of the mean magnetic field also influences the rate of convergence to the time asymptotic state, since it strongly influences the decay rate of H_m. For a small or very large value of B_0 or large H_c, convergence to the time asymptotic state could take a very long time. Thus, to obtain an accurate result in the computation of the long time averages, it was felt necessary to only begin averaging after the nonlinear decay process had eliminated the initial helicity in the system, and to choose a value of $\mathbf{B}_0$ that would result in a very rapid decay of H_m. This way transient effects associated with the decay of H_m will not bias the result. It is for this reason that we chose $\sqrt{\langle|\mathbf{b}|^2\rangle} = B_0$ for this run, because in the previous section it was shown that this value of B_0 gives the fastest decay rate for H_m. Many other simulations of the same size were performed with results not significantly different from those presented here.

In Fig. 5 the time history of H_m is given for the ideal 8^3 simulation. For this run $\mathbf{B}_0=1\hat{\mathbf{z}}$, $\sqrt{\langle|\mathbf{b}|^2\rangle}/B_0 = 1$, $E=1$, $H_c=0.2$, and at $t=0$, $H_m=0.2$. The initial spectral shape was discussed in Sec. III. This is a much longer time history than the one shown in Fig. 1(a) and serves to illustrate the fluctuating character of H_m after the nonlinear decay process has converted most of H_m into $\mathbf{B}_0\cdot\mathbf{A}_0$. This simulation is used to compute long time averages of spectral and global quantities that are compared with the absolute equilibrium theory predictions in the following section.

Before turning to the issue of the manner in which the net H_m approaches zero, it is useful to describe the way that the helicities in individual Fourier modes are distributed. A convenient measure of the polarization of the $\mathbf{b}$ fluctuations at a wave number $\mathbf{k}$ is given by $\sigma_m(\mathbf{k})=kH_m(\mathbf{k})/E_b(\mathbf{k})$, where $H_m(\mathbf{k})$ and $E_b(\mathbf{k})$ are the magnetic helicity and magnetic energy in wave number $\mathbf{k}$. A value of ± 1 for $\sigma_m(\mathbf{k})$ indicates that the fluctuations are circularly polarized, with

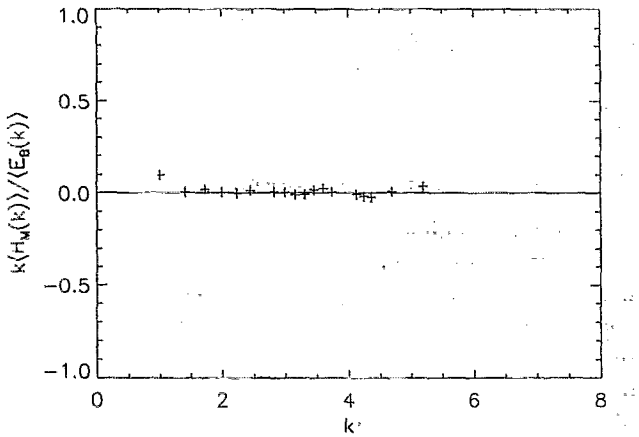

FIG. 6. Long time average of the spectrum polarization parameter $k\langle H_m(\mathbf{k})\rangle/\langle E_b(\mathbf{k})\rangle$ for the fluctuating magnetic field. This curve was obtained from averaging samples taken from the 8^3 simulation, which was integrated out to 1200 eddy turnover times.

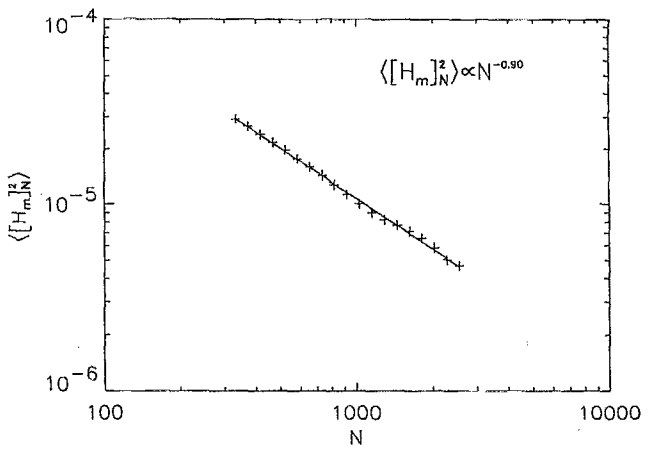

FIG. 8. Ensemble average of the square of finite time averages of length N for the H_m time history given in Fig. 5. This curve illustrates the convergence the time average of H_m to zero.

handedness determined by the sign. A value of zero indicates plane polarization. Figure 6 depicts the omnidirectional spectrum of $k\langle H_m(\mathbf{k})\rangle/\langle E_b(\mathbf{k})\rangle$. Here $\langle\cdots\rangle$ represents a time average. This quantity gives a measure of the mean polarization of the $\mathbf{b}$ fluctuations at wave numbers with magnitude k. We see that the mean polarization is near zero across the spectrum, which is consistent with the behavior of the time history of H_m depicted in Fig. 5, and suggests that the mean value of H_m is zero. This differs significantly from the $B_0=0$ case, in which H_m is conserved, and thus a nonzero mean polarization at each wave number is obtained in nondissipative simulations.[6] In Fig. 7 we show the frequency of occurrence of a particular value of $\sigma_m(\mathbf{k})$ sampled from the simulation by taking about 200 snapshots of the $\mathbf{b}(\mathbf{k})$ at times between 50 and 1200 eddy turnover times. From this figure one sees that the distribution of $\sigma_m(\mathbf{k})$ is uniform. Evidently, the nonlinear decay process destroys the net magnetic helicity in the fluctuations by taking the system to a state in which the $\mathbf{b}(\mathbf{k})$ have a polarization that is uniformly distributed with zero mean. In the following section it will be shown that this

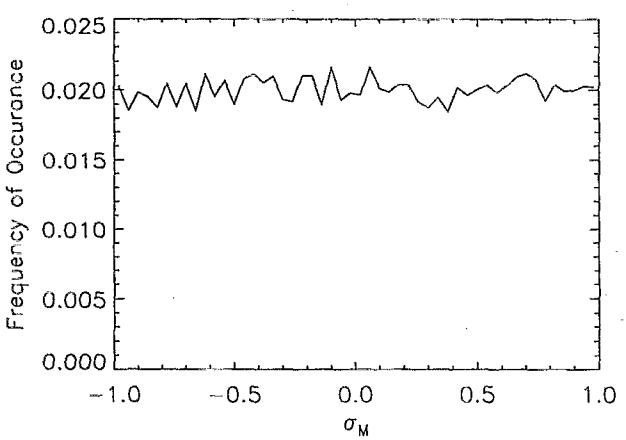

FIG. 7. Frequency of occurrence of values of $\sigma_m(\mathbf{k})=kH_m(\mathbf{k})/E_b(\mathbf{k})$ for the 8^3 ideal simulation, whose H_m time series is given in Fig. 5.

σ_m distribution over the $\mathbf{b}(\mathbf{k})$ is consistent with the $\mathbf{b}(\mathbf{k})$ having independent Gaussian distributions, with variance independent of $\mathbf{k}$ and zero mean.

To investigate the nature of the approach of H_m to zero, time averages of the H_m time series in Fig. 5 are computed. From inspection of this time series and the results presented in the previous paragraph, one would guess that it time averages to zero. To make more quantitative statements about the limit of the average as time becomes large, we must examine the time asymptotic behavior of the finite time averages. The average of H_m over a set of N points in time, with the first point located at some arbitrary position in the time series, will be denoted by $[H_m]_N$, and the average of the square of $[H_m]_N$ over many intervals of length N will be denoted by $\langle[H_m]_N^2\rangle$. For a stationary random process with zero mean,

$$\langle[H_m]_N^2\rangle\sim\frac{1}{N}, \tag{12}$$

as $N\to\infty$. A detailed account of the computation of finite interval averages from stationary random processes, and a derivation of the above relation is given in Matthaeus and Goldstein.[31] In Fig. 8, $\langle[H_m]_N^2\rangle$ for the H_m time history is given for N, ranging from 300 to 2200 corresponding to 30 to 220 eddy turnover times. The whole time series contains 12 000 points. A linear least squares fit to the curve in Fig. 8 gives $\langle[H_m]_N^2\rangle\sim N^{-0.9}$, which is acceptably close to the theoretical result, suggesting that the ensemble average $\langle H_m\rangle=0$.

The variance of the fluctuations in the H_m time history given in Fig. 5 was also computed. Because of the long correlation of the time series, we averaged the variance computed over many intervals 250 eddy turnover times in length. The correlation time, estimated from an analysis of the autocorrelation function, is approximately eight eddy turnover times. A value of 9.18×10^{-3} was found for the RMS fluctuation in H_m.

In Fig. 9 the time-averaged energy and cross-helicity spectra, and spectrum of the ratio of time-averaged kinetic energy to magnetic energy are given, averaged from 50 to

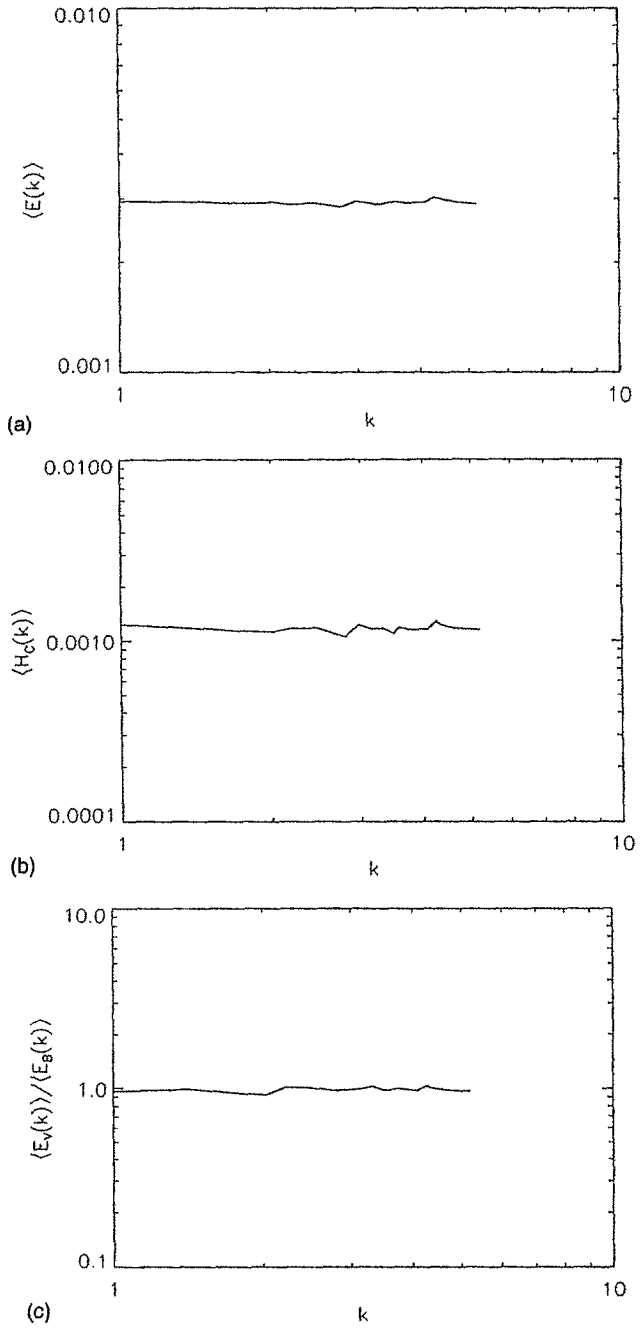

FIG. 9. Long time averages of the (a) total energy spectrum $\langle E(\mathbf{k})\rangle$, (b) cross-helicity spectrum $\langle H_c(\mathbf{k})\rangle$, and (c) the ratio of time-averaged kinetic energy to time-averaged magnetic energy $\langle E_v(\mathbf{k})\rangle/\langle E_b(\mathbf{k})\rangle$. These curves were obtained from averaging samples taken from the 8^3 simulation, which was integrated out to 1200 eddy turnover times.

1200 eddy turnover times. One can see that flat spectra are obtained with the kinetic and magnetic energy equipartitioned. Also, the global average of the ratio of kinetic to magnetic energy is 0.999 when averaged 50–1200 eddy turnover times.

As previously mentioned, our simulations suggest that the results presented here for the long time properties of this system are independent of $\mathbf{B}_0$. In the following section an absolute equilibrium theory in which only the total energy and cross-helicity are assumed as rugged invariants will be presented. It will be shown that this theory describes quite accurately the behavior observed in this inviscid simulation.

C. A possible absolute equilibrium theory

Absolute equilibrium theory has proven very successful in describing some time asymptotic properties of inviscid fluid systems, and in supplying a foundation from which qualitative conjectures are made concerning tendencies of rugged invariant spectral transfer in high Reynolds number turbulence.[1,3,6,26,27] Here we will propose an absolute equilibrium theory for 3-D MHD with a mean magnetic field that is identical in structure to the 3-D MHD theory for nonhelical magnetic fields.[6] The aspect of this theory that differs from other MHD absolute equilibrium theories[1,6,27] is that a quantity that has been identified as a quadratic invariant, namely $\hat{H}_m$, will be neglected in the construction of the absolute equilibrium ensembles. We can only give a qualitative argument to support this action. If one considers the structure of $\hat{H}_m$, see Eq. (2), it has contributions that are both local and nonlocal in time, H_m and $\mathbf{B}_0\cdot\mathbf{A}_0$, respectively. Because $\mathbf{B}_0\cdot\mathbf{A}_0$ is defined by an integral over time and $\hat{H}_m$ is an invariant in time, $\mathbf{B}_0\cdot\mathbf{A}_0$ has the property that any of its changes are a record of transient changes in H_m. In fact, the largest change in $\mathbf{B}_0\cdot\mathbf{A}_0$ occurs when the nonlinear decay process eliminates the initial H_m in the system. This suggests that $\mathbf{B}_0\cdot\mathbf{A}_0$ may be interpreted as a helicity reservoir with which the magnetic field fluctuations are in contact. Moreover, the time asymptotic value of $\hat{H}_m$ is a memory of the nonlinear decay of the initial H_m, since numerical evidence has been given to support the conjecture that H_m time asymptotically averages to zero. Hence, after a sufficiently long time the value of $\hat{H}_m$ is dynamically irrelevant.

The canonical distribution constructed assuming that E and H_c are rugged invariants has the form

$$P=\frac{1}{Z}\,e^{-(\beta E+\gamma H_c)}, \tag{13}$$

where Z is the partition function and β and γ are generalized inverse temperatures for the E and H_c, respectively. It is a simple matter to compute the ensemble-averaged E and H_c spectra, namely

$$\langle E(\mathbf{k})\rangle=\frac{4\beta}{\beta^2-\frac{1}{4}\gamma^2}, \tag{14}$$

$$\langle H_c(\mathbf{k})\rangle=-\frac{\gamma}{\beta^2-\frac{1}{4}\gamma^2}, \tag{15}$$

which are flat, and in agreement with the simulation presented in the previous section (cf. Fig. 9). The inverse temperatures are given by

$$\beta=\frac{4ME}{E^2-4H_c^2}, \tag{16}$$

$$\gamma=-4H_c\beta, \tag{17}$$

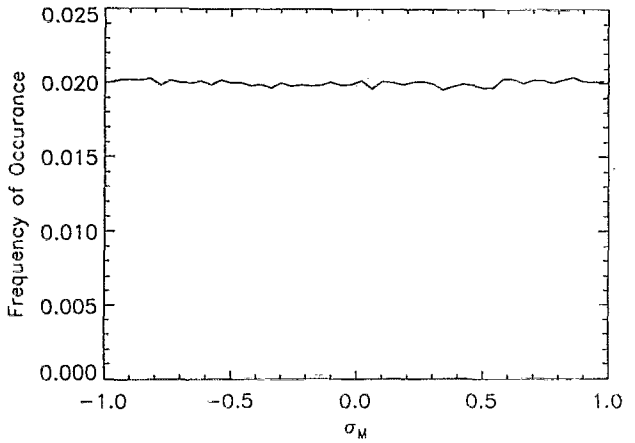

FIG. 10. Frequency of the occurrence of values of $\sigma_m(\mathbf{k})=kH_m(\mathbf{k})/E_b(\mathbf{k})$ computed from absolute equilibrium $\mathbf{b}(\mathbf{k})$ distribution. Compare with Fig. 7, which was obtained from an ideal simulation. It should also be noted that this curve is independent of the number Fourier modes M.

with M indicating the number of Fourier modes in the system. Also, the inverse temperatures must satisfy $\beta>0$ and $|\gamma|<2\beta$. The ensemble averages of the global and spectral kinetic to magnetic energy ratios are

$$\frac{\langle E_v\rangle}{\langle E_b\rangle}=1, \tag{18}$$

$$\frac{\langle E_v(\mathbf{k})\rangle}{\langle E_b(\mathbf{k})\rangle}=1, \tag{19}$$

also in agreement with the simulation presented in the previous section.

The ensemble-averaged properties of H_m are easily computed from the canonical distribution. We find that the global magnetic helicity and helicity spectrum both ensemble average to zero, both in agreement with the simulation results. The RMS fluctuation in the global value of H_m is given by

$$\sigma_{H_m}=\frac{E}{2M}\sqrt{S_M}, \tag{20}$$

$$S_M=\sum_{\mathbf{k}\in\mathbf{M}}\frac{1}{k^2}. \tag{21}$$

If the parameters of the 8^3 simulation are inserted into this expression, one obtains $\sigma_{H_m}=9.83\times10^{-3}$. This is within a few percent of 9.18×10^{-3}, which was computed from the simulation. An interesting property of Eq. (20) is that it is independent of H_c.

The absolute equilibrium version of the σ_m distribution, given in Fig. 10 for the simulation discussed in the previous section, is computed by the Monte Carlo simulation. First, the kinetic degrees of freedom are integrated over in the canonical distribution given in Eq. (13). This procedure gives the probability distribution for the $\mathbf{b}(\mathbf{k})$, which are independent identical Gaussian distributions. We then randomly generate many $\mathbf{b}(\mathbf{k})$, using this distribution, and compute $\sigma_m(\mathbf{k})$. These $\sigma_m(\mathbf{k})$ are then binned to obtain the frequency plot given in Fig. 10. This distribution is seen to be flat, and in agreement with the result obtained in the inviscid simulations.

We note in passing a curious state of affairs that presently exists with regard to the accuracy of the absolute equilibrium theory for ideal Galerkin approximations to 3-D MHD. As noted above, and in Ref. 6, spectral predictions obtained through the equilibrium theory have generally been found to be highly accurate in all cases considered. However, recently Shebalin[32] has argued that, for the case of a zero mean magnetic field, the Gibbsian statistical approach that forms the basis for these predictions may not be well founded, due to the appearance of coherent, symmetry breaking structures. Whatever the resolution of this basic issue might be for the general case, Shebalin finds no evidence for such complications for the case with a nonzero mean field. Therefore, in view of the accurate predictive capabilities of the absolute equilibrium ensemble for our current purposes, we have little reason to doubt the Gibbsian approach we have used.

D. Possible implications for dissipative flows

In the previous sections it was shown that the time-averaged properties of inviscid simulations of 3-D MHD with a mean magnetic field are consistent with an absolute equilibrium theory, in which only E and H_c are assumed as rugged invariants. The results suggest that H_m may not be a statistically isolating invariant, i.e., *nonrugged*, though it is conserved in the simulations. When H_m is a rugged invariant, i.e., in the absence of a mean magnetic field, the absolute equilibrium rugged invariant spectra have "peaks" in the longest wavelength portion. These peaks are believed to give rise to back-transfer of H_m in dissipative systems.[1] It has been shown that a nonzero mean magnetic field leads to flat time asymptotic rugged invariant spectra and a zero mean magnetic helicity spectra. These absolute equilibrium properties are identical to those obtained in nonhelical ideal 3-D MHD with no mean magnetic field.[6] Thus, the fact that H_m is no longer a rugged invariant, and furthermore decays to zero in the presence of a mean magnetic field, could have a significant impact on the nonlinear back-transfer of H_m in high Reynolds number turbulence.

Though our simulations suggest that H_m always decays to zero when a mean field is present, the time for this process to eliminate the initial H_m can be very long. We have shown that this time scale depends very strongly on both B_0 and H_c (see Sec. IV A and Figs. 3 and 4). One would anticipate that the influence of the nonlinear decay process on the evolution of a turbulent magnetofluid will depend on the separation of the nonlinear decay time scale, and possibly the magnetic helicity injection rate for forced turbulence or the energy decay time for freely decaying turbulence. If the time scale of the nonlinear H_m decay process is less than the H_m injection rate or the decay time, it is possible that H_m back-transfer will be suppressed. In the following section we will examine the effect of a mean magnetic field on freely decaying turbulence by considering the influence of an increasing mean magnetic field on the selective decay relaxation pro-

cess. Back-transfer of H_m is believed to be the mechanism that drives this relaxation process.[3]

V. MAGNETIC HELICITY DECAY PROCESS IN DECAYING FLOWS

We have shown that the presence of a mean magnetic field leads to a nonlinear magnetic helicity decay process in ideal 3-D MHD. It has also been suggested that this process may have an impact on turbulent relaxation processes, which are driven by back-transfer of magnetic helicity. In this section simulations of freely decaying 3-D MHD in a mean magnetic field will be presented. The aim of this presentation is to demonstrate that the nonlinear decay process leads to an enhanced decay rate for H_m in dissipative MHD. Also, the extent to which the selective decay and dynamic alignment relaxation process are affected by a mean magnetic field will be discussed.

We begin by examining the time evolution of H_m in a series of 32^3 simulations. In particular, we are interested in the comparison of the dissipative and nondissipative contributions to the time rate of change of H_m. The time derivative of H_m is given by

$$\frac{dH_m}{dt} = -\mathbf{B}_0 \cdot \langle \mathbf{v} \times \mathbf{b} \rangle - \eta \langle \mathbf{j} \cdot \mathbf{b} \rangle. \tag{22}$$

Here $\mathbf{j} = \nabla \times \mathbf{b}$ is the current density and $\langle \cdots \rangle$ represents a spatial average. The ideal and resistive contributions to the time derivative are $-\mathbf{B}_0 \cdot \langle \mathbf{v} \times \mathbf{b} \rangle$ and $-\eta \langle \mathbf{j} \cdot \mathbf{b} \rangle$, respectively.

Seven simulations are performed that sample the parameter space with coordinates B_0 and H_c, which are two parameters the ideal simulations suggest significantly influence the time scale of the nonlinear decay process. Six of the simulations are resistive and one is ideal. The ideal run is used a reference in determining the extent to which a nonzero resistivity and viscosity modify the nonlinear decay process. The six dissipative simulations fall into two groups. One group has an initial condition with low cross-helicity and the other high cross-helicity. The value of B_0 and the initial value of $\sqrt{\langle |\mathbf{b}|^2 \rangle}$ for the three runs in each group satisfy $B_0 = 0$, $B_0 < \sqrt{\langle |\mathbf{b}|^2 \rangle}$, and $B_0 = \sqrt{\langle |\mathbf{b}|^2 \rangle}$. Initially, in each simulation $\sqrt{\langle |\mathbf{b}|^2 \rangle} = 1$. It should also be noted that each of the three runs in a group have identical initial conditions. The only parameter different in the initial state for the three runs in each group is B_0. Thus, the runs can be compared to determine how varying B_0 changes the systems evolution. The $B_0 = 0$ runs are used as a reference for comparison with the $B_0 \neq 0$ runs, since H_m only decays because of resistivity, and because it is the system in which H_m is a rugged invariant, so that its evolution is strongly influenced by H_m back-transfer. The ideal simulations discussed in Sec. IV suggest that the nonlinear H_m decay rate is fastest when $B_0 = \sqrt{\langle |\mathbf{b}|^2 \rangle}$. In these simulations one anticipates the time scale of the nonlinear decay process to be the shortest, so if the processes is going to have a significant influence on the evolution of H_m in dissipative flows, it should be observed here. The $B_0 < \sqrt{\langle |\mathbf{b}|^2 \rangle}$ simulations are used to obtain an intermediate point in the scan of the B_0 portion of the parameter space, and to determine the smoothness of any change in the time evolution of H_m as B_0 is varied. Further details of the initial conditions and simulation parameters were discussed in Sec. III.

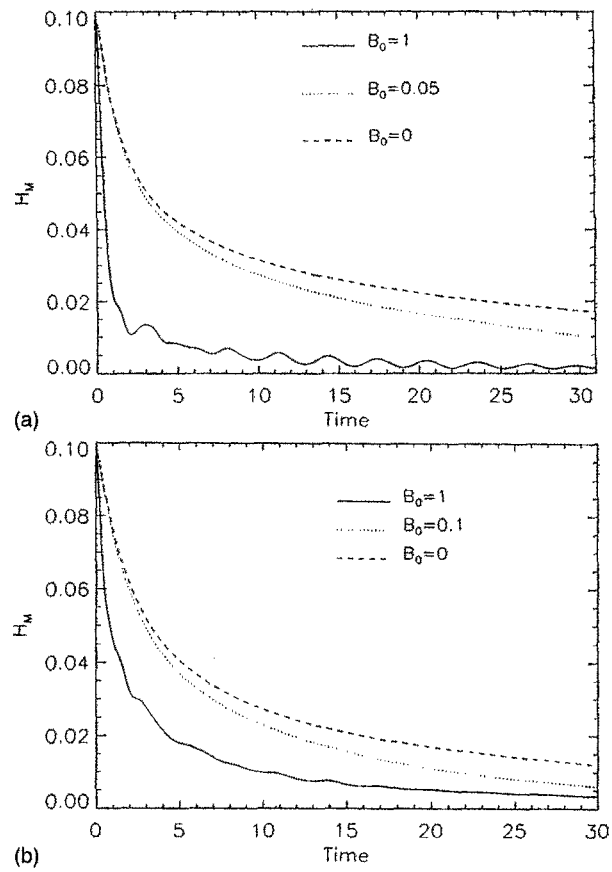

FIG. 11. Time histories of the fluctuating magnetic helicity H_m are compared for a series of 32^3 decay simulations as the magnitude of the mean magnetic field B_0 is varied. The initial conditions for $\mathbf{b}(\mathbf{k})$ and $\mathbf{v}(\mathbf{k})$ are identical for the three simulations presented in each plot. For (a) the initial condition was low in cross-helicity H_c, and in (b) the initial condition contained high H_c. The value of B_0 for each simulation is indicated in the plot.

The time history of H_m for the low H_c dissipative simulations is given in Fig. 11(a), and for the high H_c simulations in Fig. 11(b). For both cases the fastest decay rates for H_m are realized in the simulations with the largest B_0, and the slowest decay rates occur when $B_0 = 0$. If the two $B_0 = 1$ curves (solid curves) are compared between Figs. 11(a) and 11(b), one sees that the H_m decay rate is fastest for low H_c. This point is illustrated further in Fig. 12, where a plot of the time history of the ideal and resistive contributions of the H_m time derivative, see Eq. (12), $-\mathbf{B}_0 \cdot \langle \mathbf{v} \times \mathbf{b} \rangle$ and $-\eta \langle \mathbf{j} \cdot \mathbf{b} \rangle$ are given. For the low H_c simulation, Fig. 12(a), the ideal portion of the time derivative clearly dominates the resistive portion during the early stages of the simulations when H_m is decaying most rapidly. This is not true in the high H_c case, Fig. 12(b). In this simulation, the spike in $-\mathbf{B}_0 \cdot \langle \mathbf{v} \times \mathbf{b} \rangle$, the transient electric field pulse discussed in Sec. IV, is not nearly as large as in the low H_c simulation, and the resistive decay term is larger than the ideal term for the majority of the simulation. The difference in the size of $-\mathbf{B}_0 \cdot \langle \mathbf{v} \times \mathbf{b} \rangle$ can be understood in a qualitative manner, as a result of the fact

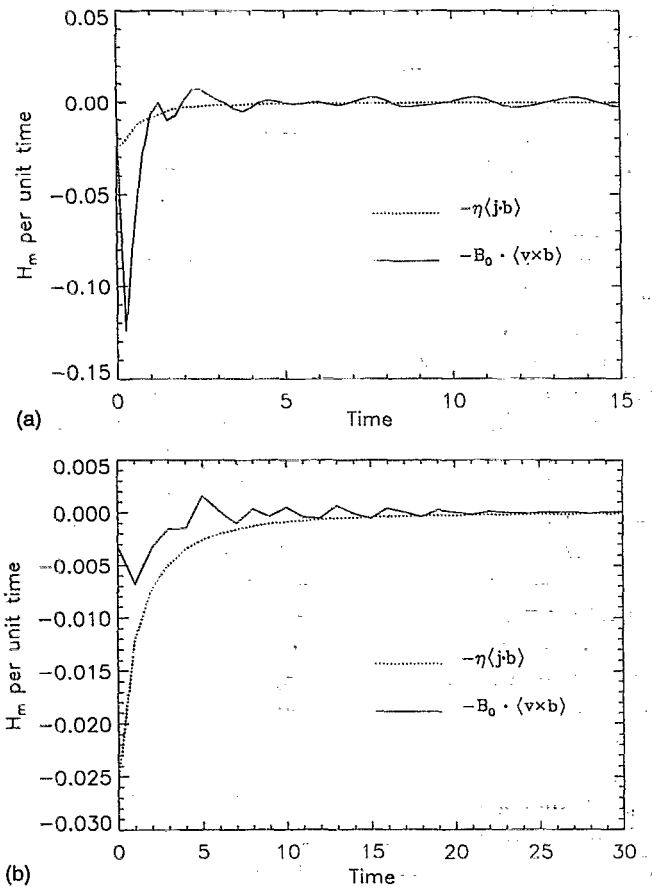

FIG. 12. Comparison of the components of the time derivative of H_m [see Eq. (22)] for two dissipative 32^3 simulations. In each plot the dotted curve is the resistive decay component $-\eta\langle \mathbf{j}\cdot\mathbf{b}\rangle$, and the solid curve is the nonlinear component $-\mathbf{B}_0\cdot\langle \mathbf{v}\cdot\mathbf{b}\rangle$. The magnitude of the mean magnetic field $B_0=1$, and initially $\sqrt{\langle|\mathbf{b}|^2\rangle}=1$ for both simulations. The initial cross-helicity H_c is low in plot (a), and high in plot (b).

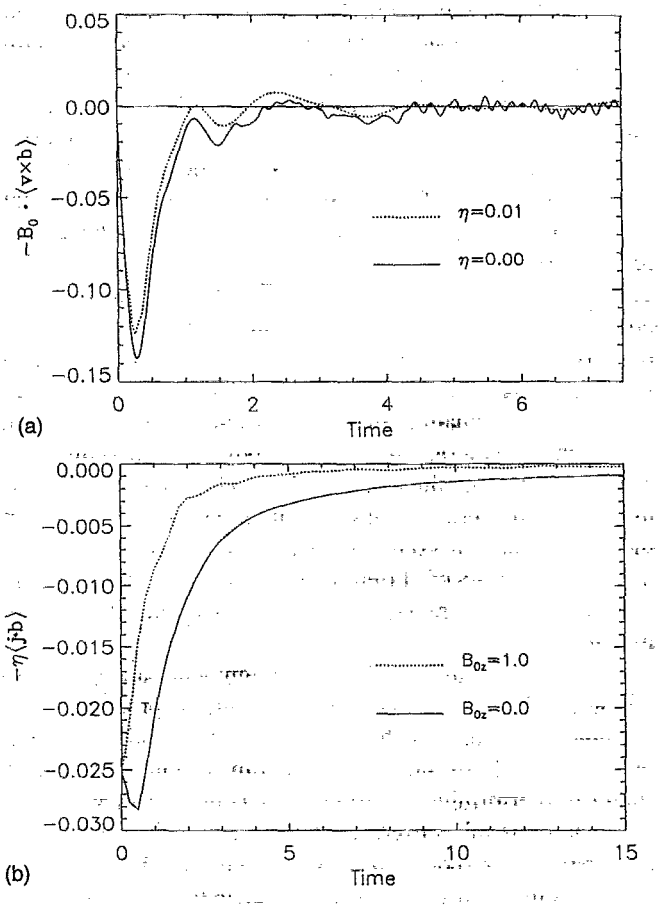

FIG. 13. In (a) the time history of the nonlinear H_m decay term [see Eq. (22)] $-\mathbf{B}_0\cdot\langle \mathbf{v}\cdot\mathbf{b}\rangle$ is compared for two 32^3 simulations with identical initial conditions, and a mean magnetic field with magnitude $B_0=1$. The dotted curve is the time history for a dissipative simulation, and the solid curve is the time history for a resistive simulation. In (b) the time history of the resistive H_m decay term $-\eta\langle \mathbf{k}j\cdot\mathbf{b}\rangle$ is compared for two 32^3 dissipative simulations with identical initial conditions. The dotted curve is the time history for a simulation with a mean magnetic field with magnitude $B_0=1$, and the solid curve is the time history for a resistive simulation with no mean magnetic field.

that increasing $|H_c|$ corresponds to increasing $|\langle \mathbf{v}\cdot\mathbf{b}\rangle|$, which should decrease $|\langle \mathbf{v}\times\mathbf{b}\rangle|$. A similar comparison in the H_m time history for low and high H_c, Figs. 11(a) and 11(b), for the other values of B_0 is not as straightforward as the previous case. In fact, it appears that the other two high H_c simulations have a slightly faster decay rate for H_m than the corresponding low H_c simulations. This seems true, even for the $B_0=0$ case. We are unable to offer a simple explanation of this result at this time.

A further comparison between the simulations is also informative. In Fig. 13(a) the time histories of $-\mathbf{B}_0\cdot\langle \mathbf{v}\times\mathbf{b}\rangle$ for the $B_0=1$ low H_c simulation and the ideal 32^3 simulation are compared. Both of these simulations have the same initial condition. The two curves follow each other very closely. The slight difference is most likely the result of damping of high-frequency oscillations by dissipation and a rescaling of the curve for the dissipative simulation caused by decay of the total energy. This result suggests that the nonlinear H_m decay process is, for the most part, unmodified by nonzero dissipation, or at least when $B_0 \sim \sqrt{\langle|\mathbf{b}|^2\rangle}$ and H_c low. In Fig. 13(b) the time histories of $-\eta\langle \mathbf{j}\cdot\mathbf{b}\rangle$ for the $B_0=1$ and $B_0=0$ low H_c simulations and are compared. It can be seen that the resistive component of dH_m/dt is smaller for the $B_0=1$ simulation, even though H_m decays at a faster rate [see Fig. 11(a)]. The suppression of the resistive component of dH_m/dt in this simulation is possibly also a consequence of the nonlinear decay process, since $\langle \mathbf{j}\cdot\mathbf{b}\rangle$ is just a k^2 weighted sum over the H_m spectrum. A similar result, though not shown, is obtained in the high H_c simulations, but with an anticipated smaller difference between the two curves, since the time scale of the nonlinear decay process is longer [see Fig. 12(b)].

VI. EFFECT ON TURBULENT RELAXATION PROCESSES

In the previous section it was shown that the nonlinear decay process presented in Sec. IV leads to a faster decay rate for H_m in dissipative MHD than would occur by resistive decay alone. In this section it will be shown that the nonlinear decay process can decreases the time scale for H_m decay to a sufficient extent to extinguish selective decay relaxation.

In 3-D MHD turbulent decay with no DC magnetic field different directions and time scales for the nonlinear spectral transfer of the rugged invariants give rise to inequalities in their decay rates. These decay rate inequalities drive a decaying system toward a state of minimum energy as time becomes infinite. Back-transfer of magnetic helicity to low wave numbers, and forward transfer of total energy to high wave numbers lead to a faster decay rate for total energy relative to magnetic helicity.[3] This relaxation process has been referred to as selective decay.[12] Selective decay relaxation takes the decaying fluid from an arbitrary initial condition toward a large-scale magnetically force-free state. A faster decay rate for cross-helicity relative to total energy, referred to as dynamic alignment, occurs as well. Dynamic alignment relaxation takes the decaying magnetofluid to a state of Alfvénic fluctuations. Several dynamical mechanisms for this process have been proposed.[29,30,33,34] Each mechanism has in common that the decay rate inequality develops because of different or equal time scales for the forward spectral transfer of positive and negative cross-helicity.

Selective decay and dynamic alignment can operate simultaneously in a decaying magnetofluid to produce a time asymptotic state, which exhibits characteristics of both processes.[7,35] The properties of this time asymptotic state are found by performing a variational calculation in which the total energy is minimized, while the cross-helicity and magnetic helicity are constrained to be constants. For a 3-D periodic geometry with $k_{\min}=1$, this calculation yields[7]

$$\left(\frac{H_m}{E_b}\right)_\infty = \pm 1, \tag{23}$$

$$\left(\frac{H_c}{\sqrt{E_v E_b}}\right)_\infty = \pm 1. \tag{24}$$

A decaying magnetofluid approaches a state that satisfies both of these equations as time becomes infinite for any initial condition that contains sufficient H_m and H_c.[7] Equation (23) is a consequence of the magnetic helicity constraint in the variational calculation, and reflects the fact that the time asymptotic state is large scale and magnetically force-free, i.e., $\mathbf{b}=\nabla\times\mathbf{b}$. Equation (24) indicates that the fluctuating velocity and magnetic fields are aligned, and is due to the cross-helicity constraint in the variational calculation. The time asymptotic kinetic to magnetic energy ratio is given by

$$\left(\frac{E_v}{E_b}\right)_\infty = \frac{2}{\sigma_{c\infty}^2} - 1 - \sqrt{\left(\frac{2}{\sigma_{c\infty}^2} - 1\right)^2 - 1}, \tag{25}$$

where $\sigma_{c\infty}$ is the time asymptotic value of $2H_c/E$. Notice also, that $(E_v/E_b)_\infty < 1$ for all $\sigma_{c\infty}$, and that $(E_v/E_b)_\infty \to 0$ as $\sigma_{c\infty}\to 0$ and $(E_v/E_b)_\infty \to 1$ as $\sigma_{c\infty}\to \pm 1$ Unlike Eqs. (23) and (24), which are satisfied independently of the initial condition, Eq. (25) depends on the initial condition in an unknown way, since there is no known way to compute the time asymptotic value $\sigma_{c\infty}$, other than estimating it by direct numerical simulation. Experience gained from simulations tells us that if the initial value of H_c is small, then $\sigma_{c\infty}$ is generally small, so that $(E_v/E_b)_\infty \approx 0$, and if H_c is large then $(E_v/E_b)_\infty$ is usually about unity.[7]

In the remainder of this section we will discuss simulations that investigate how the nonlinear H_m decay process effects selective decay and dynamic alignment relaxation. The parameters H_m/E_b, $H_c/\sqrt{E_v E_b}$, and E_v/E_b will be computed from the simulation, and the degree of convergence to the time asymptotic values predicted by the theories will be used to qualitatively estimate the extent to which the system has selectively decayed or dynamically aligned. We will compare these parameters for simulations with a mean magnetic field of varying magnitude. Two simulations, one with low H_c and the other high H_c, in which $B_0=0$ will be used as a reference for comparison with the $B_0\neq 0$ simulations. In the $B_0=0$ system, both H_m and H_c are rugged invariants, so it is anticipated that both selective decay and dynamic alignment relaxation will occur. For the $B_0\neq 0$ system only H_c is a rugged invariant, and thus one will only expect dynamic alignment relaxation. However, it is possible that if the time scale for the nonlinear helicity decay process is sufficiently long compared to the energy decay time, some properties of selective decay relaxation may nonetheless characterize the systems evolution. Divergence between the selective decay relaxation parameters as time increases for the $B_0=0$ and the $B_0\neq 0$ simulations will give indications of the extent to which the nonlinear decay process has interfered with H_m back-transfer in the freely decaying system. The series of six decay simulations previously mentioned will also be used in the following discussion.

First, we will examine the evolution of the low cross-helicity set of simulations. For the $B_0=0$ case, one would expect an evolution dominated by selective decay, because the initial condition is low in H_c. In the H_m/E-$2H_c/E$ parameter space classification proposed in Ref. 7, one anticipates a region I type evolution. Initial conditions that lie in this portion of the parameter space are characterized by $|H_m|/E_b$ increasing in time, and approaching unity as time becomes large. The system should also become magnetic energy dominated as time increases, i.e., $E_v \ll E_b$. In Fig. 14, where the time histories of H_m/E_b and E_v/E_b for the low H_c simulations are compared, this is indeed what is seen for the $B_0=0$ simulation (a dashed line). For this simulation H_m/E_b rapidly increases from its initial value to near 0.9 when time integration ceased, and E_v/E_b decreases for the duration of the simulation. When time integration stopped, E_b is nearly 20 times greater than E_v.

When $B_0\neq 0$ one first notices from Fig. 14(a) that the rate of increase of H_m/E_b decreases as B_0 increases, and from Fig. 14(b) one sees that as B_0 increases E_v and E_b become increasingly equipartitioned. However, the time histories of H_m/E_b and E_v/E_b for the weak B_0 simulation (the dotted lines in Fig. 14) very closely track the $B_0=0$ simulation for a significant length of time. Though the simulation began with B_0 much less than $\sqrt{\langle|\mathbf{b}|^2\rangle}$, resistivity eventually produces $\sqrt{\langle|\mathbf{b}|^2\rangle} \approx B_0$, which, in turn, decreases the time scale of the nonlinear decay process, and thus the curves begin to diverge. Rapid divergence of H_m/E_b for the two simulations begins at about ten turnover times when

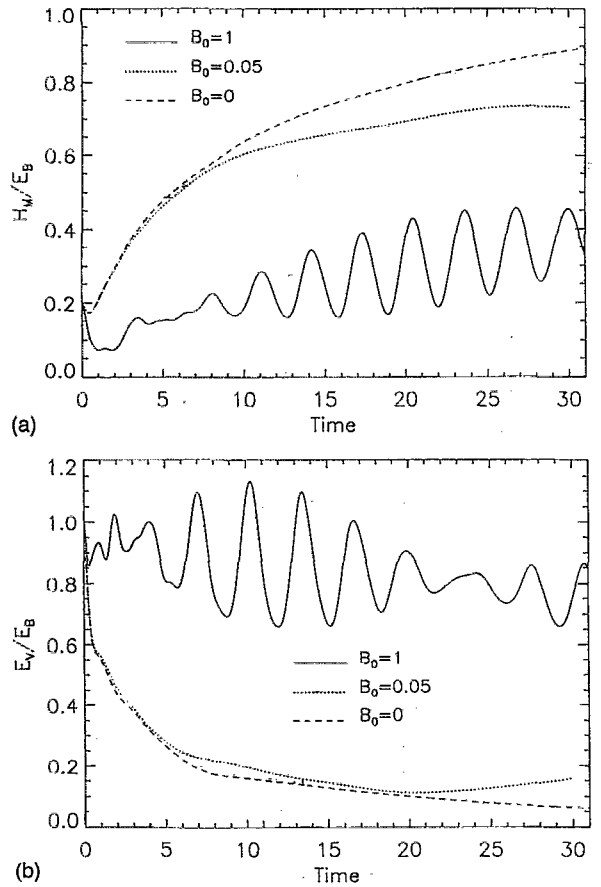

FIG. 14. Low cross-helicity 32^3 runs with identical initial conditions, but varying mean magnetic field B_0. Time histories of (a) H_m/E_b and (b) E_v/E_b.

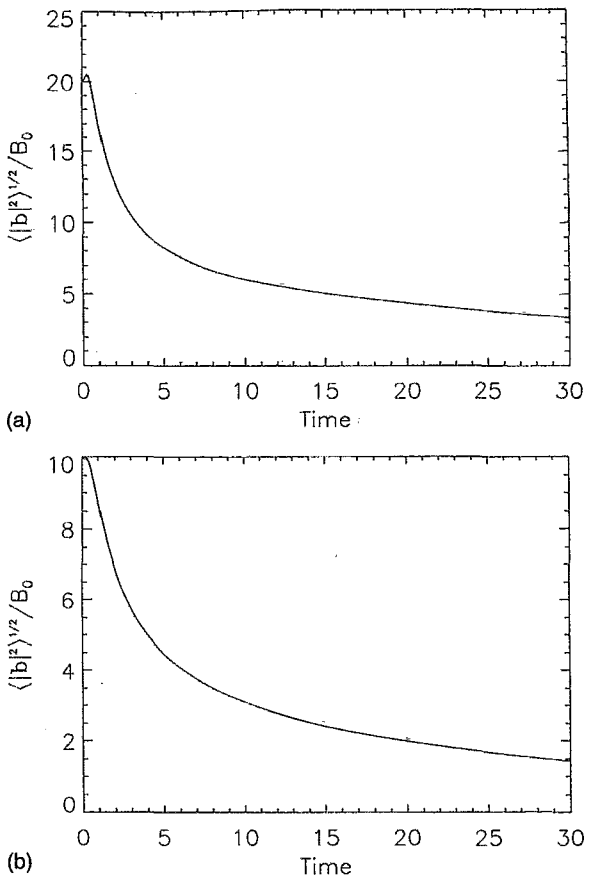

FIG. 15. Time history of the parameter $\sqrt{\langle|\mathbf{b}|^2\rangle}/B_0$ for two dissipative simulations, one with high cross-helicity H_c (a) and one with low H_c (b).

$\sqrt{\langle|\mathbf{b}|^2\rangle}/B_0 \approx 5$ (see Fig. 15). The E_v/E_b curves do not begin to separate until nearly 20 turnover times. At this latter time, $\sqrt{\langle|\mathbf{b}|^2\rangle}/B_0$ is still approximately 5, After divergence of the curves, the rate of increase in H_m/E_b for the weak B_0 simulation appears to be slowing down, and possibly asymptoting at a value less than the minimum energy value of unity. While E_v/E_b for the same simulation is showing signs of continuing to increase, contrasting the selective decay scenario of evolution.

In the simulation with $\sqrt{\langle|\mathbf{b}|^2\rangle} = B_0$ initially, H_m/E_b (a solid curve) is always much less than in the $B_0=0$ simulation, and never exhibits any characteristics of evolution in the selective decay scenario. Dissipation leads to a decrease in $\sqrt{\langle|\mathbf{b}|^2\rangle}/B_0$ as time advances, causing the linear wave term in Eq. (3) to dominate the evolution of the system. This produces oscillations at approximately the Alfvén period of structures approximately half the wavelength of the largest scales propagating in $\mathbf{B}_0$. Just as H_m/E_b for this run failed to follow a selective decay type of evolution, so too did E_v/E_b [the solid curve Fig. 14(b)]. In Fig. 14(b) one sees the E_v/E_b oscillates about $E_v \approx E_b$ for the entire simulation. Thus, when we initially have $\sqrt{\langle|\mathbf{b}|^2\rangle} \approx B_0$, the helicity decay process prevents the appearance of characteristics of H_m backtransfer in a freely decaying magnetofluid.

Now consider the set of high H_c simulations, the results of which are presented in Figs. 15–17. For the $B_0=0$ case this set of simulations contains sufficient initial values of H_c and H_m to produce an evolution characterized by both the selective decay and dynamic alignment processes. For this case, we expect "region II" behavior,[7] characterized $|H_m|/E_b$ and $|H_c|/\sqrt{E_v E_b}$ increasing and approaching unity at long times. The time asymptotic value of E_v/E_b is given by Eq. (25), once $\sigma_{c\infty}$ is determined by simulation. The time history of H_m/E_b, E_v/E_b, and $H_c/\sqrt{E_v E_b}$ are given for the $B_0=0$ simulation by the dashed curves in the three panels of Fig. 16, which verify the expected behavior. The estimate of $\sigma_{c\infty}$ from the simulation is 0.94 (see the dashed curve, Fig. 17). Inserting this into Eq. (25) gives $(E_v/E_b)_\infty=0.49$, which is consistent with the time history given in Fig. 16(b). This $B_0=0$ simulation provides a basis for the discussion of the nonzero B_0 cases.

For the weak B_0, high H_c simulation [the dotted curve in Figs. 16(a) and 16(b)], the time histories of H_m/E_b and E_v/E_b behave similarly to the weak B_0 low H_c simulation. At early times both cases closely follow their $B_0=0$ counterparts, and show nonzero B_0 effects once the fluctuation amplitude reduces to $\sqrt{\langle|\mathbf{b}|^2\rangle}/B_0 \approx 5$ (see Fig. 15). After this time H_m/E_b increases at a much slower rate, apparently asymptoting at a value less than the minimum energy value of unity and E_v/E_b begins to increase. This indicates that selective decay-type evolution becomes disfavored.

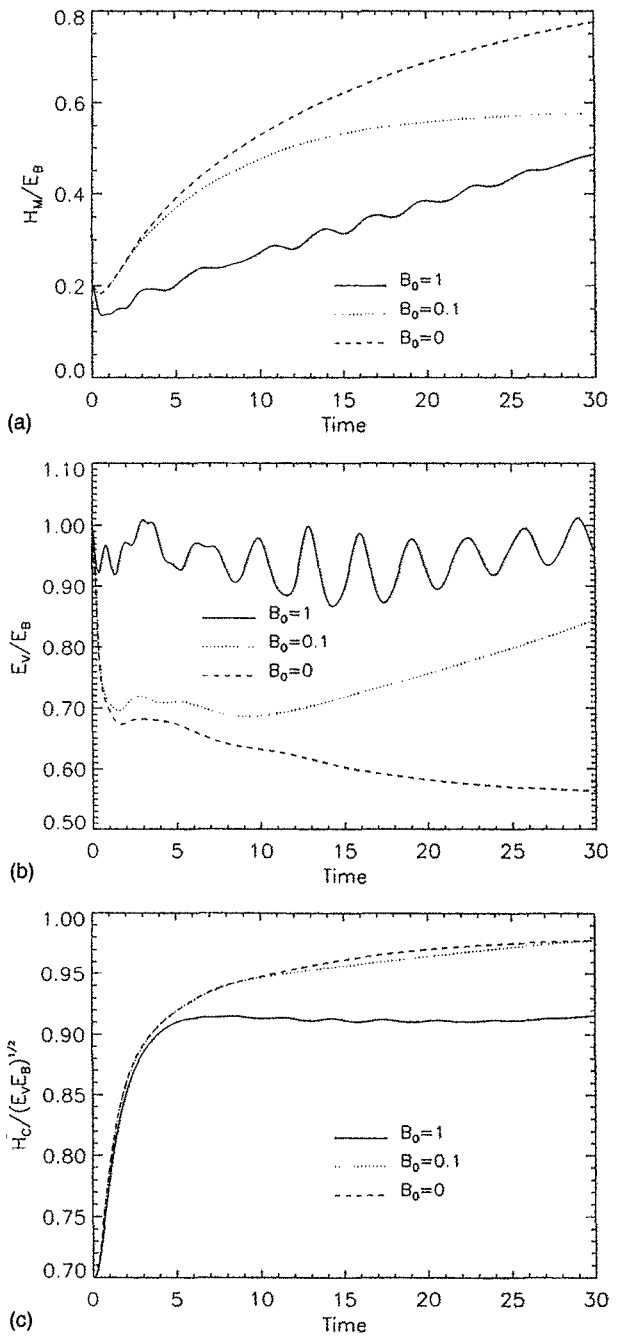

FIG. 16. Comparison of time histories of (a) H_m/E_b, (b) E_v/E_b, and (c) $H_c/\sqrt{E_vE_b}$, as the magnitude of the mean magnetic field B_0 is varied for three 32^3 dissipative simulations with a high cross-helicity initial condition.

For strong B_0 and high H_c, the evolution H_m/E_b and E_v/E_b [the solid curve, Figs. 16(a) and 16(b)] can be qualitatively compared to the similar low H_c run in Fig. 14. In each case the effect of nonzero B_0 is to cause a much slower rate of growth of H_m/E_b than in the respective $B_0=0$ simulations. The time history of E_v/E_b oscillates about unity for the entire simulation in both cases. These characteristics differ considerably from the $B_0=0$ selective decay process.

Because the runs shown in Fig. 16 contain initially large cross-helicity, we can also examine the influence of helicity decay and strength of B_0 on the dynamic alignment relaxation process. In a number of theories, H_m back-transfer is not needed to produce dynamic alignment[29,30,33,34] (however, see Refs. 6 and 7). Moreover, H_c remains a rugged invariant when $B_0\neq 0$, so one might think that dynamic alignment is not substantially affected by the nonlinear H_m decay process or the value of B_0. Our simulations indicate that this may not be the case. Instead we find what appears to be a quite complex dependence on the magnitude of the mean magnetic field.

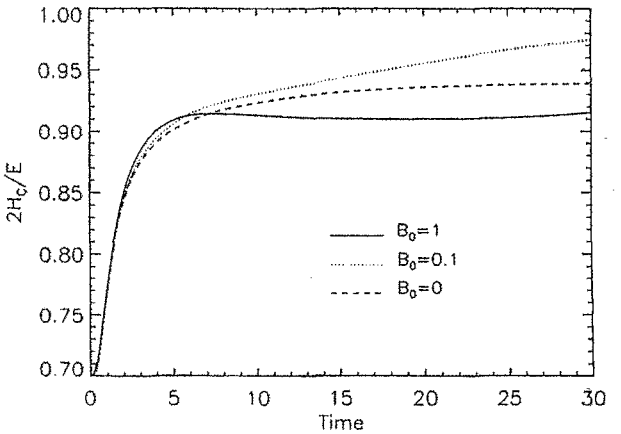

FIG. 17. Comparison of the time history of $2H_c/E$ as the magnitude of the mean magnetic field B_0 is varied for three 32^3 dissipative simulations.

Dynamic alignment properties of the runs with nonzero B_0 can be seen in Fig. 16(c) and in Fig. 17, where a constrast can be made with the similar $B_0=0$ run. Time evolution of $H_c/\sqrt{E_vE_b}$ (the mean cosine between the velocity and magnetic fields), in Fig. 16(c), shows the $B_0=0$ simulation, following a typical dynamic alignment scenario. The weak B_0 simulation (a dashed line) follows the $B_0=0$ simulation very closely; both cases show $H_c/\sqrt{E_vE_b}$, increasing from 0.7 to near 0.98 during the runs. Near the beginning of the simulation, the strong B_0 curve [the solid line in Fig. 16(c)] follows both the $B_0=0$ and weak B_0 curves very closely, but after about five eddy turnover times the strong B_0 curve diverges very rapidly from the other two. From eight to the end of the simulation, the strong B_0 curve changes very little. This curve is apparently asymptoting at approximately 0.915, a value less than that expected for a minimum energy state.

Further insight into the dynamic alignment behavior of these runs in seen in Fig. 17, which gives time histories of $2H_c/E$. This parameter measures the relative decay rates of H_c and E, and is not sensitive to changes in the partition of kinetic and magnetic energy, as is $H_c/\sqrt{E_vE_b}$. Dynamic alignment results from a slower decay rate for H_c relative to E. A system evolving along the dynamic alignment scenario should, at early times, experience rapid growth in $2H_c/E$. At later times the growth rate should slow as the minimum energy value is approached. This is exactly the behavior seen in the $B_0=0$ simulation [the dashed curve in Fig. 16(c)]. In fact, the value read from this plot at 30 eddy turnover times was used in Eq. (25) to estimate the time asymptotic value of E_v/E_b, which favorably compared with the simulation result.

The $B_0\neq 0$ behavior of $2H_c/E$ is quite different. First,

for the strong B_0 simulation (the solid curve in Fig. 17), $2H_c/E$ behaves very similarly to $H_c/\sqrt{E_v E_b}$ [Fig. 16(c)], which is a consequence of equipartition of kinetic and magnetic energy [see the solid curve in Fig. 16(b)]. However, the inferred final state is not a minimum energy energy state, compatible with constraints of constant H_m or H_c that have been previously identified.[6,7] It appears that the evolution that would lead to dynamic alignment has been "frozen out," and that no significant further activity in $2H_c/E$ or $H_c/\sqrt{E_v E_b}$ will occur. This may be a consequence of the nonlinear decay of H_m, and also of B_0, but it is not anticipated that the mere slowing of nonlinear transfer associated with a mean magnetic field can produce this effect.

For the weak B_0 case, Fig. 17 shows that $2H_c/E$ (the dotted line) has grown to a large value, but it is unclear whether it is asymptoting to a value less than the upper bound of unity. There are two possibilities for the subsequent evolution of this simulation. First, in view of the fact that E_v/E_b is increasing [Fig. 16(b)] while $H_c/\sqrt{E_v E_b}$ is approaching unity [Fig. 16(c)], this run may be approaching the special region of parameter space designated as region III in earlier work on decay with $B_0=0$.[7] This state is obtained theoretically by considering only the cross-helicity constraint, which has the time asymptotic properties $E_v=E_b$ and $2H_c/E=1$.[7] The second possibility for the continued evolution of this simulation is that its $2H_c/E$ evolution could "freeze out" in the manner described above for the strong B_0 simulation. If this were the case then it is possible that a continuum of time asymptotic states exists. Clearly, a delicate balance of effects is at work in this interesting region of parameter space. Here H_m decay is slow, as is nonlinear spectral transfer. It is unclear which constraints are most effective in determining the properties of the long time decaying state of the system. Examination of these effects will require a more extensive parameter space scan than the one reported here.

VII. SUMMARY AND CONCLUSIONS

We have given a survey of the consequences of change in nondissipative invariance from fluctuation magnetic helicity H_m [see Eq. (1)] to modified fluctuation magnetic helicity $\hat{H}_m$ [see Eq. (2)] on the dynamics of 3-D MHD turbulence in the presence of a uniform magnetic field. First, the evolution of $\hat{H}_m$ in ideal 3-D MHD with a mean magnetic field was discussed. It was shown by numerical simulation the $\hat{H}_m$ is a constant in time for this system. Also, the conservation of $\hat{H}_m$ was shown to give rise to a nonlinear process, which led to the conversion of the initial magnetic helicity in the fluctuating magnetic field H_m into magnetic helicity, measured by the quantity $2\mathbf{B}_0\cdot\mathbf{A}_0$ [see Eq. (2)]. A precise interpretation of the magnetic helicity defined by $\mathbf{B}_0\cdot\mathbf{A}_0$ requires further work, but some insights may be gained by arriving at the homogeneous model through a multiple length scale analysis (e.g., see Ref. 18).

After sufficient time the nonlinear process is believed to produce a state in which H_m fluctuates about zero and $2\mathbf{B}_0\cdot\mathbf{A}_0$ fluctuates about the initial value of H_m while conserving $\hat{H}_m$. The time scale of this process was shown to vary with both the magnitude of the mean magnetic field B_0 and the cross-helicity H_c. A minimum value for the time scale as a function of B_0 is thought to occur when $B_0 \approx \sqrt{\langle|\mathbf{b}|^2\rangle}$. For weaker B_0, the nonconservation of H_m is not felt as strongly, whereas for stronger B_0 the nonlinear couplings are weakened, which delays all nonlinear effects, including H_m decay. As H_c is increased toward its maximum value of $\pm\frac{1}{2}E$, the time scale also increases. The conversion of H_m to $2\mathbf{B}_0\cdot\mathbf{A}_0$ by the nonlinear process generates a mean electric field parallel to the mean magnetic field. Properties of this electric field pulse were deduced from the conservation of $\hat{H}_m$ and its definition.

The long time average properties of ideal simulations were discussed. After a sufficiently long time, the nonlinear H_m decay process was shown to produce a steady state that has no average H_m. The properties of this state also appear to be independent of B_0. Spectrally, H_m was shown to be consistent with Gaussian zero mean $\mathbf{b}(\mathbf{k})$ fluctuations, with random polarization having a zero mean and a uniform distribution. Other properties of this state are total energy and cross-helicity spectra that are equipartitioned in wave number, as well as equipartition spectrally and globally between the kinetic and magnetic energy. An absolute equilibrium theory was constructed, which only assumed the total energy and cross-helicity are isolating invariants. This model compared favorably with the long time averages computed from the simulations. This absolute equilibrium theory is identical in structure to one describing nonhelical MHD without a mean magnetic field.[6,32] The invariance in time of $\hat{H}_m$ was ignored in the construction of the equilibrium theory. It was suggested that the nonisolating character of $\hat{H}_m$ may arise from its nonlocality in time.

It was previously mentioned that the study of the statistical mechanics of ideal MHD formed the base from which qualitative predictions about nonlinear spectral transfer tendencies in high Reynolds number MHD turbulence are made. In 3-D MHD with no mean magnetic field, where H_m is a rugged invariant, sharp peaks occur in the longest wavelength of the absolute equilibrium H_m spectrum. The total energy and cross-helicity are also peaked at the longest wavelength, but not to the degree of H_m. It is believed that this structure of the rugged invariant spectra gives rise to the back-transfer of H_m in dissipative MHD.[1] We have shown that the presence of a mean magnetic field leads to flat ensemble-averaged rugged invariant spectra, and zero ensemble-averaged H_m spectrum. Thus, one is led to suggest that the presence of a mean magnetic field may suppress H_m back-transfer effects in MHD turbulence if the time scale for the nonlinear decay of H_m is sufficiently fast. For freely decaying MHD, the nonlinear decay of H_m may inhibit selective decay relaxation, since it is believed to be driven by the back-transfer of H_m.[3]

In the simulations of freely decaying 3-D MHD presented in Secs. V and VI, we found that the presence of a mean magnetic field caused a faster rate of decay of H_m than resistivity alone. If initially $B_0 \approx \sqrt{\langle|\mathbf{b}|^2\rangle}$ the nonlinear decay process dominated resistive decay. For an initially strong B_0, this enhanced H_m decay rate was shown to eliminate selective decay-type evolution, indicating the suppression of

H_m back-transfer in the system's dynamics. For systems that had an initially weak mean magnetic field, early evolution was characterized by features of selective decay, but at later times the systems diverged from this trajectory, showing no clear signs of approaching a selective decay time asymptotic state. This result suggests that the nonlinear H_m decay process has a negative impact on H_m back-transfer, regardless of the initial strength of the applied uniform magnetic field.

The simulation results presented in Sec. IV give indications that dynamic alignment relaxation may be suppressed by the presence of a strong B_0 as well. The simulation beginning with $B_0 \approx \sqrt{\langle |\mathbf{b}|^2 \rangle}$ did not give indications that it would time asymptotically approach the dynamically aligned state. However, the weak B_0 simulation was possibly headed toward the dynamically aligned time-asymptotic state. The mechanism for possible quenching of dynamic alignment in the strong B_0 regime is not well understood, and may relate to effects of both H_m decay and other influences of B_0.

In a previous brief report of this work,[18] we proposed a simple phenomenology for the nonlinear H_m decay process. The model captures the essential feature of the process, such as the decay of H_m and the concurrent electric field pulse. In the model the process has a form reminiscent of an α dynamo from mean field electrodynamics.[19] It is shown that $\mathbf{E}_0 \approx -\alpha \mathbf{B}_0$, where for the freely decaying system α is a functional of H_m, which depends upon time. If H_m is injected into the system at some constant rate, then when averaged over time, α is constant, and a mean electric field parallel to $\mathbf{B}_0$ is maintained. In the construction of this model, it was necessary to introduce time scales associated with the spectral transfer time of the electric field and an Alfvén time associated with H_m. Work is in progress to develop a better understanding of the these time scales, and to try to compute them from simulation data. Also, there are plans to perform simulations, where magnetic helicity is injected. In this system the nonlinear H_m decay process may give rise to a stationary mean electric field parallel to the applied uniform magnetic field, whose properties may also be described by the simple phenomenological model.

ACKNOWLEDGMENTS

The authors would like to thank S. Ghosh, D. Montgomery, M. L. Goldstein, and D. A. Roberts for helpful discussions. Computations were performed at the National Aeronautics and Space Administration Center for Computational Sciences at the Goddard Space Flight Center and at the National Science Foundation San Diego Supercomputer Center.

This work was funded by the National Research Council and the National Aeronautics and Space Administration Solar Terrestrial Theory Program Grants at the Goddard Space Flight Center and at Bartol.

[1] U. Frisch, A. Pouquet, J. Léorat, and A. Mazure, J. Fluid Mech. **68**, 769 (1975).
[2] A. Pouquet, U. Frisch, and J. Léorat, J. Fluid Mech. **77**, 321 (1976).
[3] D. Montgomery, L. Turner, and G. Vahala, Phys. Fluids **21**, 757 (1978).
[4] A. Pouquet and G. S. Patterson, J. Fluid Mech. **85**, 305 (1978).
[5] S. Riyopoulos, A. Bondeson, and D. Montgomery, Phys. Fluids **25**, 107 (1982).
[6] T. Stribling and W. H. Matthaeus, Phys. Fluids B **2**, 1979 (1990).
[7] T. Stribling and W. H. Matthaeus, Phys. Fluids B **3**, 1848 (1991).
[8] M. Meneguzzi, U. Frisch, and A. Pouquet, Phys. Rev. Lett. **47**, 1069 (1981).
[9] J. B. Taylor, Phys. Rev. Lett. **33**, 1139 (1974).
[10] R. Horiuchi and T. Sato, Phys. Fluids **29**, 1161 (1986).
[11] H. K. Moffatt, *Magnetic Field Generation in Electrically Conducting Fluids* (Cambridge University Press, Cambridge, 1978).
[12] W. Matthaeus and D. Montgomery, Ann. NY Acad. Sci. **357**, 202 (1980).
[13] W. H. Matthaeus and M. L. Goldstein, J. Geophys. Res. **87**, 6011 (1982).
[14] M. L. Goldstein, D. A. Roberts, and C. A. Fitch, Geophys. Res. Lett. **18**, 1505 (1991).
[15] J. W. Bieber, P. Evenson, and W. H. Matthaeus, Astrophys. J. **315**, 700 (1987).
[16] J. W. Bieber, P. Evenson, and W. H. Matthaeus, Geophys. Res. Lett. **14**, 864 (1987).
[17] J. W. Bieber and C. W. Smith, EOS **73**, 247 (1992).
[18] T. Stribling, W. H. Matthaeus, and S. Ghosh, J. Geophys. Res. **99**, 2567 (1994).
[19] F. Krause and K.-H. Rädler, *Mean Field Electrodynamics and Dynamo Theory* (Pergamon, New York, 1980).
[20] Y. Zeldovich, A. Ruzmaikin, and D. Sokoloff, *Magnetic Fields in Astrophysics* (Gordon and Breach, New York, 1983).
[21] R. H. Kraichnan, J. Fluid Mech. **67**, 155 (1975).
[22] R. H. Kraichnan, J. Fluid Mech. **67**, 155 (1975).
[23] S. A. Orszag, Stud. Appl. Math. **50**, 293 (1971).
[24] L. C. Kells and S. A. Orszag, Phys. Fluids **21**, 162 (1977).
[25] T. D. Lee, Qt. Appl. Math. **10**, 69 (1952).
[26] R. H. Kraichnan, Phys. Fluids **10**, 1417 (1967).
[27] D. Fyfe and D. Montgomery, J. Plasma Phys. **16**, 181 (1976).
[28] R. H. Kraichnan, Phys. Fluids **8**, 1385 (1965).
[29] W. H. Matthaeus and Y. Zhou, Phys. Fluids B **1**, 1929 (1989).
[30] R. Grappin, U. Frisch, J. Léorat, and A. Pouquet, Astron. Astrophys. **105**, 6 (1982).
[31] W. H. Matthaeus and M. L. Goldstein, J. Geophys. Res. **87**, 10 347 (1982).
[32] J. V. Shebalin, Phys. Plasmas **1**, 541 (1994).
[33] M. Dobrowolny, A. Mangeney, and P. L. Veltri, Phys. Rev. Lett. **45**, 144 (1980).
[34] W. H. Matthaeus, M. L. Goldstein, and D. Montgomery, Phys. Rev. Lett. **51**, 1484 (1983).
[35] A. C. Ting, W. H. Matthaeus, and D. Montgomery, Phys. Fluids **29**, 3261 (1986).